Received: 27 March 2024 | Revised: 5 June 2024 | Accepted: 8 June 2024

DOI: 10.1111/mmi.15291

RESEARCH ARTICLE

WILEY

# Cleavage of an engulfment peptidoglycan hydrolase by a sporulation signature protease in *Clostridioides difficile*

Diogo Martins[1] | Hailee N. Nerber[2] | Charlotte G. Roughton[3] | Amaury Fasquelle[1] | Anna Barwinska-Sendra[3] | Daniela Vollmer[3,4] | Joe Gray[3] | Waldemar Vollmer[3,4,5] | Joseph A. Sorg[2] | Paula S. Salgado[3,4] | Adriano O. Henriques[1] | Mónica Serrano[1]

[1]Instituto de Tecnologia Química e Biológica António Xavier, Universidade Nova de Lisboa, Oeiras, Portugal

[2]Biology Department, Texas A&M University, College Station, Texas, USA

[3]Faculty of Medical Sciences, Biosciences Institute, Newcastle University, Newcastle upon Tyne, UK

[4]Faculty of Medical Sciences, Biosciences Institute, Centre for Bacterial Cell Biology, Newcastle University, Newcastle upon Tyne, UK

[5]Institute for Molecular Bioscience, The University of Queensland, St Lucia, Brisbane, Australia

**Correspondence**
Mónica Serrano and Adriano O. Henriques, Instituto de Tecnologia Química e Biológica António Xavier, Universidade Nova de Lisboa, Avenida da República EAN, 2780-157 Oeiras, Portugal.
Email: serrano@itqb.unl.pt and aoh@itqb.unl.pt

**Funding information**
Fundação para a Ciência e a Tecnologia, Grant/Award Number: LISBOA-01-0145-FEDER-007660, PD/BD/143148/2019 and PTDC/BIA-MIC/29293/2017; Medical Research Council, Grant/Award Number: MR/V032151/1; Biotechnology and Biological Sciences Research Council, Grant/Award Number: BB/W013630/1 and BB/W005557/1; Barbour Foundation PhD Studentship; National Institute of Allergy and Infectious Diseases, Grant/Award Number: R01AI116895 and R01AI172043; European Union Marie Sklodowska Curie Innovative Training Networks, Grant/Award Number: 642068

## Abstract

In the model organism *Bacillus subtilis*, a signaling protease produced in the forespore, SpoIVB, is essential for the activation of the sigma factor $\sigma^K$, which is produced in the mother cell as an inactive pro-protein, pro-$\sigma^K$. SpoIVB has a second function essential to sporulation, most likely during cortex synthesis. The cortex is composed of peptidoglycan (PG) and is essential for the spore's heat resistance and dormancy. Surprisingly, the genome of the intestinal pathogen *Clostridioides difficile*, in which $\sigma^K$ is produced without a pro-sequence, encodes two SpoIVB paralogs, SpoIVB1 and SpoIVB2. Here, we show that *spoIVB1* is dispensable for sporulation, while a *spoIVB2* in-frame deletion mutant fails to produce heat-resistant spores. The *spoIVB2* mutant enters sporulation, undergoes asymmetric division, and completes engulfment of the forespore by the mother cell but fails to synthesize the spore cortex. We show that SpoIIP, a PG hydrolase and part of the engulfasome, the machinery essential for engulfment, is cleaved by SpoIVB2 into an inactive form. Within the engulfasome, the SpoIIP amidase activity generates the substrates for the SpoIID lytic transglycosylase. Thus, following engulfment completion, the cleavage and inactivation of SpoIIP by SpoIVB2 curtails the engulfasome hydrolytic activity, at a time when synthesis of the spore cortex peptidoglycan begins. SpoIVB2 is also required for normal late gene expression in the forespore by a currently unknown mechanism. Together, these observations suggest a role for SpoIVB2 in coordinating late morphological and gene expression events between the forespore and the mother cell.

Hailee N. Nerber and Charlotte G. Roughton contributed equally to this work.

**KEYWORDS**
cortex, peptidoglycan, serine-protease, SpoIIP, SpoIVB

## 1 | INTRODUCTION

*Clostridioides difficile* is an obligate anaerobic intestinal pathogen (Abt et al., 2016; Smits et al., 2016). It has the ability to differentiate into endospores (referred to as spores), and it uses these oxygen-resistant cells for environmental persistence and transmission (Deakin et al., 2012; Smits et al., 2014). Spores consist of a central compartment, the core, which holds the genome and is delimited by the spore's inner membrane. This unit is surrounded by a layer of PG called the germ cell wall (GCW), which will become the cell wall of the vegetative cell upon germination and outgrowth. A much thicker PG layer, the cortex, essential for heat resistance, surrounds the GCW and is formed between the inner and outer spore membranes. Surrounding the cortex are two proteinaceous layers, the coat and the exosporium, that protect against PG-degrading enzymes and are the first line of contact of the spore with the environment (Gil et al., 2017; Henriques & Moran, 2007).

During sporulation, the forespore and the mother cell maintain different programs of gene expression. These programs, however, are coordinated by cell–cell communication pathways involving the production of signaling proteins that are either secreted or reside in the membranes that delimit either cell. Despite variations in the signaling pathways that regulate sporulation in *C. difficile* and the *Bacillus subtilis* model (Fimlaid et al., 2013; Hilbert & Piggot, 2004; Pereira et al., 2013; Saujet et al., 2013), they enforce the fidelity of spore differentiation in both organisms.

In *B. subtilis*, the RNA polymerase sigma factor $\sigma^G$ becomes active in the forespore after engulfment completion. The $\sigma^G$-controlled production of a signaling serine protease, SpoIVB, in the forespore and its secretion into the intermembrane space leads to activation of a membrane-associated pro-sigma factor, pro-$\sigma^K$, in the mother cell (Sun et al., 2021). SpoIVFB is the protease that converts pro-$\sigma^K$ to its transcription-competent form; SpoIVFB is embedded in the membrane but kept inactive in a complex with SpoIVFA and BofA (Olenic et al., 2022). Cleavage of SpoIVFA by SpoIVB in the intermembrane space causes a conformational change in SpoIVFB, which can then cleave pro-$\sigma^K$, to release active $\sigma^K$ (De Hoon et al., 2010; Eichenberger et al., 2004; Ramírez-Guadiana et al., 2018). *B. subtilis* SpoIVB has another substrate, the forespore-specific SpoIIQ protein (Chiba et al., 2007; Jiang et al., 2005). SpoIIQ plays a role in PG remodeling events that are central to engulfment but are also needed for the localization of proteins required for the post-engulfment activation of gene expression in the forespore, through $\sigma^G$, and in the mother cell, through $\sigma^K$ (Doan et al., 2005; Londoño-Vallejo et al., 1997; Rodrigues et al., 2013). Following engulfment completion, SpoIIQ is cleaved by SpoIVB but this event is not essential for sporulation (Chiba et al., 2007).

Apart from triggering pro-$\sigma^K$ activation, SpoIVB plays another essential role in sporulation (Oke et al., 1997; Wakeley et al., 2000) as certain missense mutations in *spoIVB* prevent the formation of the cortex PG layer and, hence, the production of heat resistant spores, while not eliminating pro-$\sigma^K$ processing. The molecular basis of this phenotype is unknown.

Remarkably, the *C. difficile* genome codes for two developmentally regulated SpoIVB paralogs, SpoIVB1 and SpoIVB2, yet $\sigma^K$ is produced without an inhibitory pro-sequence (Fimlaid et al., 2013; Pereira et al., 2013; Serrano, Kint, et al., 2016). This raised the possibility that *C. difficile* has segregated the different functions of *B. subtilis* SpoIVB into two different proteins. To understand the role of the two SpoIVB paralogs of *C. difficile*, we constructed and characterized in-frame deletion mutants for the two genes. We found that *spoIVB1*, the *C. difficile* counterpart of *B. subtilis spoIVB*, is dispensable for the formation of heat resistant spores. *spoIVB2*, however, is essential for sporulation and the mutant was unable to form the cortex PG layer and showed impaired late forespore-specific gene expression.

No SpoIIQ cleavage product was detected in *C. difficile* (Ribis et al., 2018). However, we found that SpoIIP, an amidase/endopeptidase essential for PG remodeling during engulfment, undergoes site-specific processing by SpoIVB2. Importantly, cleavage of SpoIIP by SpoIVB2 abolishes the enzymatic activity of the protein leading us to propose that, upon completion of engulfment, the PG hydrolytic activity required during engulfment, is abrogated.

## 2 | RESULTS

### 2.1 | *C. difficile* has two *spoIVB* homologs

*C. difficile* encodes two *spoIVB* homologs (Abecasis et al., 2013; Galperin et al., 2012; Traag et al., 2013), *spoIVB1*, which is encoded just upstream of *spo0A*, a transcription factor essential for entry into sporulation (Deakin et al., 2012; Rosenbusch et al., 2012; Smits et al., 2014), and *spoIVB2*, localized between *fisB*, that encodes a protein essential for membrane fission at the end of engulfment, and *lytH*, coding for a PG hydrolase involved in cortex maturation (Doan et al., 2013; Horsburgh et al., 2003) (Figure 1a). *B. subtilis spoIVB* is also upstream of *spo0A*, suggesting that *spoIVB1* is its counterpart in *C. difficile* (Figure 1a). To gain structural insight into the three SpoIVB proteins, we used AlphaFold2 (AF2), together with the Foldseek server (Jumper et al., 2021; Mirdita et al., 2022; van Kempen et al., 2024) (Figure 1b). The model generated for *B. subtilis* SpoIVB (hereinafter $SpoIVB^{Bs}$) suggests that, in addition to the transmembrane helix that targets the protein to the intermembrane space, $SpoIVB^{Bs}$ consists of three independent structural domains: an immunoglobulin-like (Ig-like) domain (residues 31–101), a PDZ domain (residues 120–186), and the serine

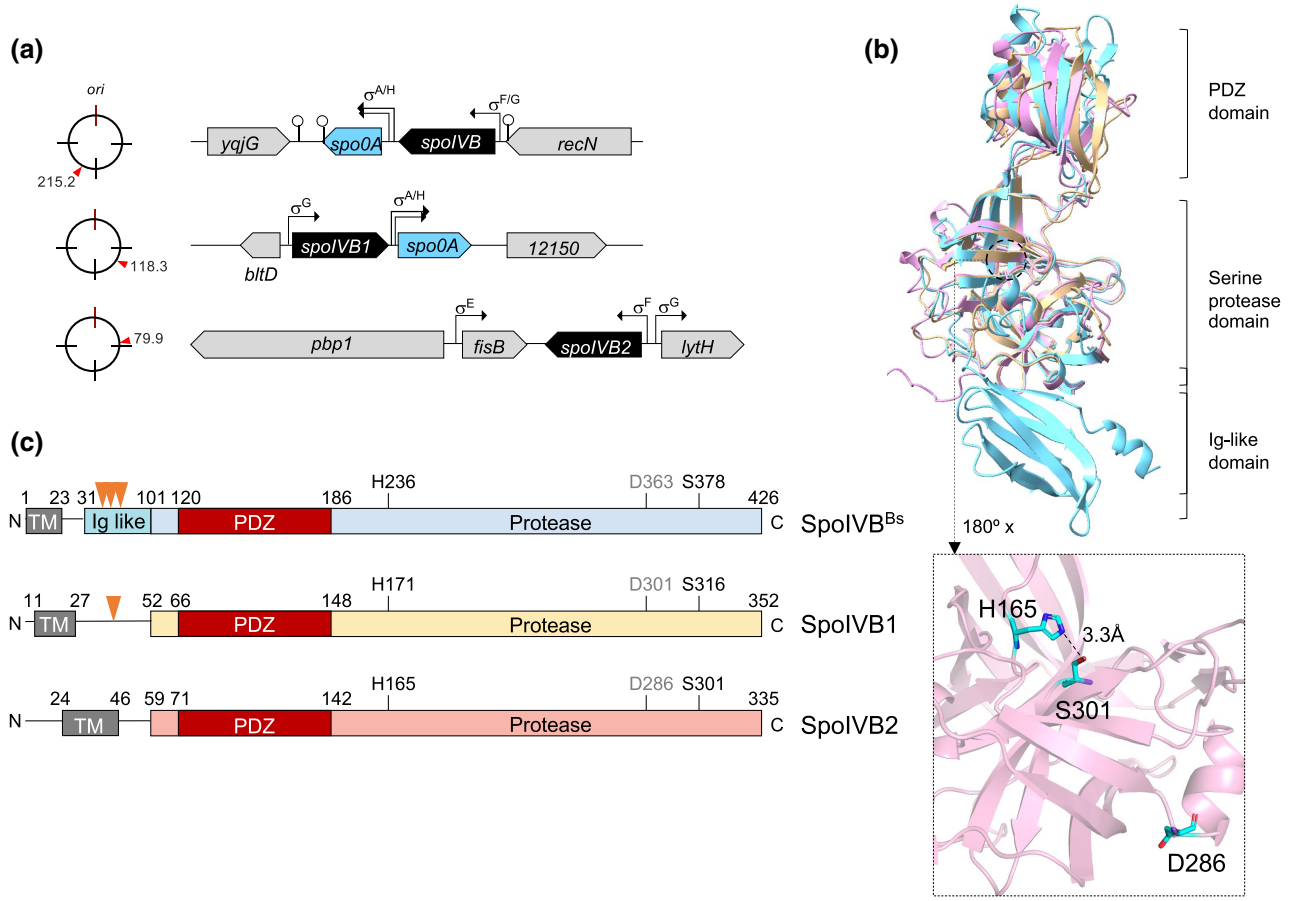


**FIGURE 1** The *spoIVB* chromosomal context and domain organization of the SpoIVB proteins. (a) Genetic map of the *spoIVB* regions of the *Bacillus subtilis* (top) and *Clostridioides difficile* (bottom) chromosomes. Promoters are represented by broken arrows and the sigma factors that utilize them are indicated; transcription terminators are symbolized by stem and loop structures. *C. difficile* possesses two *spoIVB* paralogs. We named *spoIVB1* the gene in synteny with its *B. subtilis* counterpart (close to *spo0A*), while *spoIVB2* is flanked by *lytH* and *fisB*. (b) Superimposed AF2-generated models of SpoIVB$^{Bs}$, SpoIVB1, and SpoIVB2 without the transmembrane helices (top). The color code matches that of panel c, except for the PDZ domain. The bottom panel shows an expansion of the active site region of SpoIVB2 to show the relative positions of His165, Asp286, and Ser301. (c) Domain organization of the SpoIVB proteins. The SpoIVB protein of *B. subtilis* (SpoIVB$^{Bs}$) shows an immunoglobulin (Ig) like N-terminal domain, a PDZ domain, essential for substrate binding and cleavage, and the serine protease domain, which harbors the catalytic residues. SpoIVB1 and SpoIVB2 share a high degree of sequence similarity with SpoIVB$^{Bs}$ in the PDZ and the serine protease domains but lack the Ig-like domain. Predicted transmembrane regions (TM) are represented. The orange arrowheads represent cleavage sites identified in SpoIVB$^{Bs}$ and predicted in SpoIVB1. The residues proposed to form the catalytic triad are indicated above the diagrams (His165, Asp286, and Ser301, for SpoIVB2).

protease domain (residues 186–426). SpoIVB$^{Bs}$ self-cleavage at the Ig-like domain (at residues Asn53, Phe63, and Thr75) releases the active protease to the intermembrane space (Wakeley et al., 2000). Earlier work suggested that the catalytic triad is formed by His236, Ser378, and Asp363 (Hoa et al., 2002) (Figure 1c). According to the AF2 model, however, Asp363 is distant from His236 and Ser378, and may not be involved in catalysis. A structure determined by small-angle X-ray scattering (SAXS) of an enzymatically inactive form of SpoIVB$^{Bs}$ encompassing residues Thr75 to Ser426 fused to a modified MBP (mMBP), mMBP-SpoIVB$^{BsS378A}$, shows the proposed three active site residues distant from each other and divergently oriented (Xie et al., 2019). The serine protease domain may thus adopt a zymogen-like inactive conformation (Xie et al., 2019).

Both *C. difficile* SpoIVB1 and SpoIVB2 lack the Ig-like domain and the transmembrane helices are followed by the PDZ and serine protease domains (Figure 1b,c). SpoIVB1 shows a conserved autocleavage site at Phe42 (Figures 1c and 6c), suggesting that, like SpoIVB$^{Bs}$, it may be released into the intermembrane space. In contrast, SpoIVB2 lacks residues resembling the SpoIVB$^{Bs}$ self-cleavage or signal peptidase sites, and it may remain membrane-associated. As in SpoIVB$^{Bs}$, the proposed catalytic triads of SpoIVB1 and SpoIVB2 do not seem properly oriented for catalysis according to the AF2 predicted models (Figure 1c).

## 2.2 | *spoIVB2*, but not *spoIVB1*, is required for sporulation

To analyze the function of the two *C. difficile* SpoIVB proteins, we started by constructing in-frame deletion mutants in the *C. difficile*

630Δ*erm* strain using allele-coupled exchange (Ng et al., 2013) (Figure S1). We found that the *spoIVB1* mutant produces heat-resistant spores to the same level as the wild-type strain (WT; Figure 2a). In contrast, no heat-resistant spores were detected for the *spoIVB2* mutant (Figure 2a). Phase contrast microscopy of samples withdrawn from sporulation medium (70:30 medium agar plates) after growth and sporulation for 24 h showed that most cells of the *spoIVB2* mutant are blocked after engulfment completion (53%; Figure 2b,c). Interestingly, phase-gray spores were often released as immature "sporelets" (40%; Figure 2b,c). Analysis of the *spoIVB2* mutant by transmission electron microscopy (TEM) showed many sporangia of immature forespores that lacked the cortex layer while showing deposition of some coat/exosporium material (Figures 2d and S2). This phenotype was fully complemented by the expression of a WT allele of *spoIVB2* from a multicopy plasmid but not by an allele coding for a catalytic inactive protease (*spoIVB2*$^{S301A}$) (Figures 2a,d and S2), confirming the requirement of SpoIVB2 activity for sporulation. The multicopy

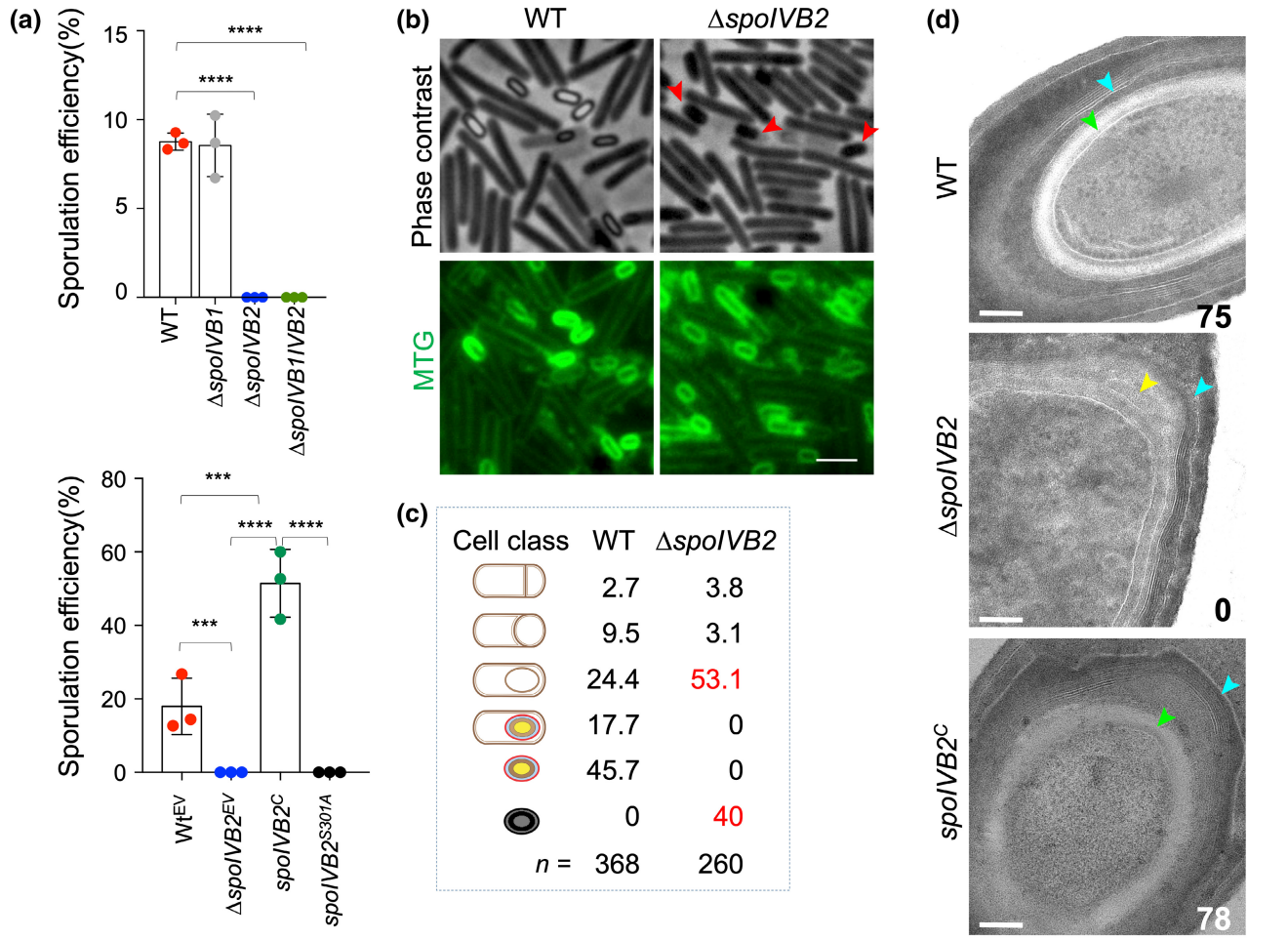


**FIGURE 2** *spoIVB2* is required for sporulation. (a) Sporulation efficiency for the indicated strains. In the bottom panel, the strains carry the following plasmids: EV, empty vector; C, plasmid with the WT *spoIVB2* allele; S301A, plasmid carrying the *spoIVB2*$^{S301A}$ allele. Strains were incubated in 70:30 medium for 24 h and the cultures were plated in BHI medium supplemented with 0.1% taurocholate (TA) before (to estimate total CFUs mL$^{-1}$) and after heat treatment at 70°C for 30 min (spores mL$^{-1}$). The results shown are averages and standard deviations for three biological replicates. Asterisks indicate statistical significance determined with a two-way ANOVA (***$p < 0.001$; ****$p < 0.0001$). (b) Phase contrast and fluorescence images of sporulating cells of the WT and a congenic *spoIVB2* mutant. The cells were collected after incubation for 24 h in a 70:30 sporulation medium and stained with the membrane dye MTG. Note that the *spoIVB2* mutant does not produce phase bright spores, although sporangia of phase gray spores and free "sporelets" are seen. Scale bar, 2 μm. (c) Scoring of the percentage of cells in each of the morphological classes of sporulation (from top to bottom): soon after asymmetric division; during engulfment; just after engulfment completion; sporangia of phase bright spores; free phase bright spores and free phase dark spores, as assessed by phase contrast and fluorescence microscopy for the indicated strains after 24 h of incubation on 70:30 plates. The percentage of cells in each class is relative to the number of sporulating cells; "*n*" is the total number of sporulating cells scored. (d) Thin sectioning transmission electron microscopy of the WT, *spoIVB2* mutant and the mutant complemented in trans (*spoIVB2*$^{C}$). Samples were taken after incubation for 24 h (as in a) and processed for TEM. In the *spoIVB2* mutant, engulfment is completed and coat/exosporium material is deposited around the forespore (blue arrowhead) but the cortex layer, (green arrowhead in the WT), is absent (the yellow arrow points to the cortex region in the mutant). Cortex formation is restored in the complemented strain. The numbers refer to the percentage of sporulating cells exhibiting coat/exosporium and cortex layers around the forespore. See also Figure S2. Scale bar, 0.2 μm.

allele of WT *spoIVB2* consistently increases the sporulation efficiency (Figure 2a). The reason for this is unclear but one possibility is that the cloned DNA titrates an inhibitor of sporulation or alternatively that the normal levels of SpoIVB2 are limiting for sporulation. In any event, a double *spoIVB1/spoIVB2* mutant mimics the *spoIVB2* single mutant (Figure 2a).

Previous work has shown that *spoIVB1* and *spoIVB2* are both expressed in the forespore, *spoIVB1* under $\sigma^G$ control and *spoIVB2* under the control of $\sigma^F$ (Pereira et al., 2013). Accordingly, SpoIVB1 would accumulate later than SpoIVB2 during sporulation, which could explain why *spoIVB1* does not compensate for the absence of *spoIVB2*. To test this, we placed *spoIVB1* under the control of the *spoIVB2* promoter. However, we were not able to detect heat-resistant spores in this strain, indicating that *spoIVB1* is unable to replace *spoIVB2*, regardless of time of expression (Figure 3a).

The phenotype of the *spoIVB2* mutants is similar to that of *B. subtilis spoIVB* mutants that bypass the need for SpoIVB signaling in the activation of pro-$\sigma^K$ but not the second function of the protein (Oke et al., 1997; Wakeley et al., 2000). Since $\sigma^K$ lacks a pro-sequence in *C. difficile*, SpoIVB2 could have the second function of $SpoIVB^{Bs}$, that is, in cortex synthesis. In *B. subtilis*, the $spoIVB^{T228A}$ allele enables signaling leading to partial activation of pro-$\sigma^K$, but not cortex synthesis (Oke et al., 1997). Residue Thr228 is conserved in SpoIVB2 (Thr157) but not in SpoIVB1 (Met163) (Figure 3b). To test whether Thr157 is important in SpoIVB2, plasmid-born $spoIVB2^{T157M}$ and $spoIVB1^{M163T}$ alleles were introduced in a *spoIVB2* mutant. The allele coding for $SpoIVB1^{M163T}$ was not able to restore sporulation to a *spoIVB2* mutant (Figure 3a). In contrast, the allele coding for $SpoIVB2^{T157M}$ restored the production of phase bright heat-resistant spores, to levels significantly higher than the WT (Figure 3a). Thus, contrary to what was observed in *B. subtilis*, Thr157 is not essential for the function of SpoIVB2, although it may somehow control the activity of the protein.

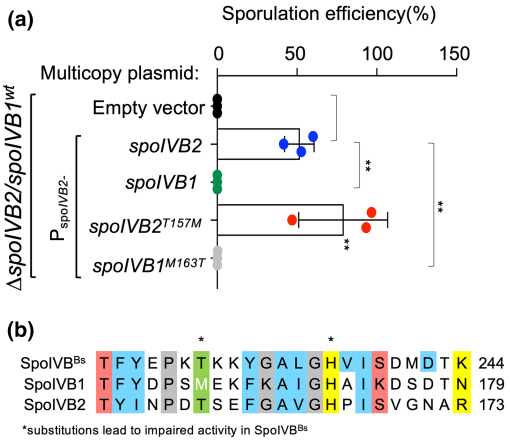


**FIGURE 3** *spoIVB1* does not complement the *spoIVB2* mutant. (a) Sporulation efficiency for the indicated strains. Strains were incubated in a 70:30 sporulation medium for 24 h and samples were plated onto BHI plates containing 0.1% TA before and after heat treatment at 70°C for 30 min. The results shown are averages and standard deviations for three biological replicates. Asterisks indicate statistical significance determined with a two-way ANOVA (**$p < 0.01$). (b) The alignment shows a region of the SpoIVB proteins which includes an amino acid, Thr228, that when replaced by Ala, blocks sporulation in *Bacillus subtilis*, while allowing signaling of pro-$\sigma^K$ processing. This residue is conserved in SpoIVB2 (Thr157) but not in SpoIVB1 (Met163).

## 2.3 | *spoIVB2* is required for normal late forespore-specific gene expression

The *C. difficile sigG* mutant is blocked following engulfment completion and the cortex is absent, while some coat/exosporium material accumulates around the forespore (Fimlaid et al., 2013; Pereira et al., 2013). This phenotype is similar to that of the *spoIVB2* deletion mutant, prompting us to test whether gene expression during sporulation was affected in the mutant. We first monitored the activity of $\sigma^F$ and $\sigma^E$ using transcriptional fusions of the *gpr* and *spoIIIA* promoters, respectively, to the $SNAP^{Cd}$ reporter (Pereira et al., 2013). After 14 h of incubation on the sporulation medium, the expression of $P_{gpr}$-$SNAP^{Cd}$ was detected in 46% of the sporulating cells of the WT and the *spoIVB2* mutant (Figure 4a). Expression of $P_{spoIIIA}$-$SNAP^{Cd}$ was detected in 84% of the sporulating cells in the WT and 88% of the *spoIVB2* sporangia (Figure 4a). Moreover, the average intensity of the fluorescence signal from the $P_{gpr}$- and $P_{spoIIIA}$-$SNAP^{Cd}$ fusions of the WT or *spoIVB2* mutant was similar (Figure 4b). Kolmogorov–Smirnov test analysis showed a significant difference in the distribution of the fluorescence intensity in individual cells carrying $P_{gpr}$-$SNAP^{Cd}$, with the *spoIVB2* mutant showing a subpopulation of cells with high intensity (Figure 4b).

To monitor the activity of $\sigma^G$ and $\sigma^K$, we used previously characterized $P_{sspA}$-$SNAP^{Cd}$ and $P_{cotE}$-$SNAP^{Cd}$ transcriptional fusions, respectively (Pereira et al., 2013). Expression of $P_{sspA}$-$SNAP^{Cd}$ was detected exclusively in the forespore, in 86% of the WT sporangia, and in 82% of the *spoIVB2* sporangia (Figure 4c). The intensity of the fluorescence signal per cell, however, was significantly lower in the *spoIVB2* mutant (Figure 4d). In contrast, no difference was observed in the intensity of the fluorescence signal from $P_{cotE}$-$SNAP^{Cd}$ between the WT and the *spoIVB2* mutant (Figure 4c,d), but the number of cells expressing $P_{cotE}$-$SNAP^{Cd}$ was higher in the mutant (83%) than in the WT (55%). This may be due to the accumulation of sporulating cells at late stages of sporulation because of a block in morphogenesis. This could also explain the subpopulation of cells with an increased $P_{gpr}$-$SNAP^{Cd}$ signal (see also below). The fact that $\sigma^K$ activity is detected in the *spoIVB2* mutant is consistent with the deposition of coat/exosporium material around the forespore, as these layers become visible by TEM in a $\sigma^K$-dependent manner (see Pereira et al., 2013).

Another gene under $\sigma^G$ control is *spoVT*, coding for an ancillary transcription factor that together with $\sigma^G$ turns on the expression of *sspA* and *sspB* (Pereira et al., 2013). A *spoVT* mutant produces phase dark heat sensitive "sporelets" with no (or reduced)

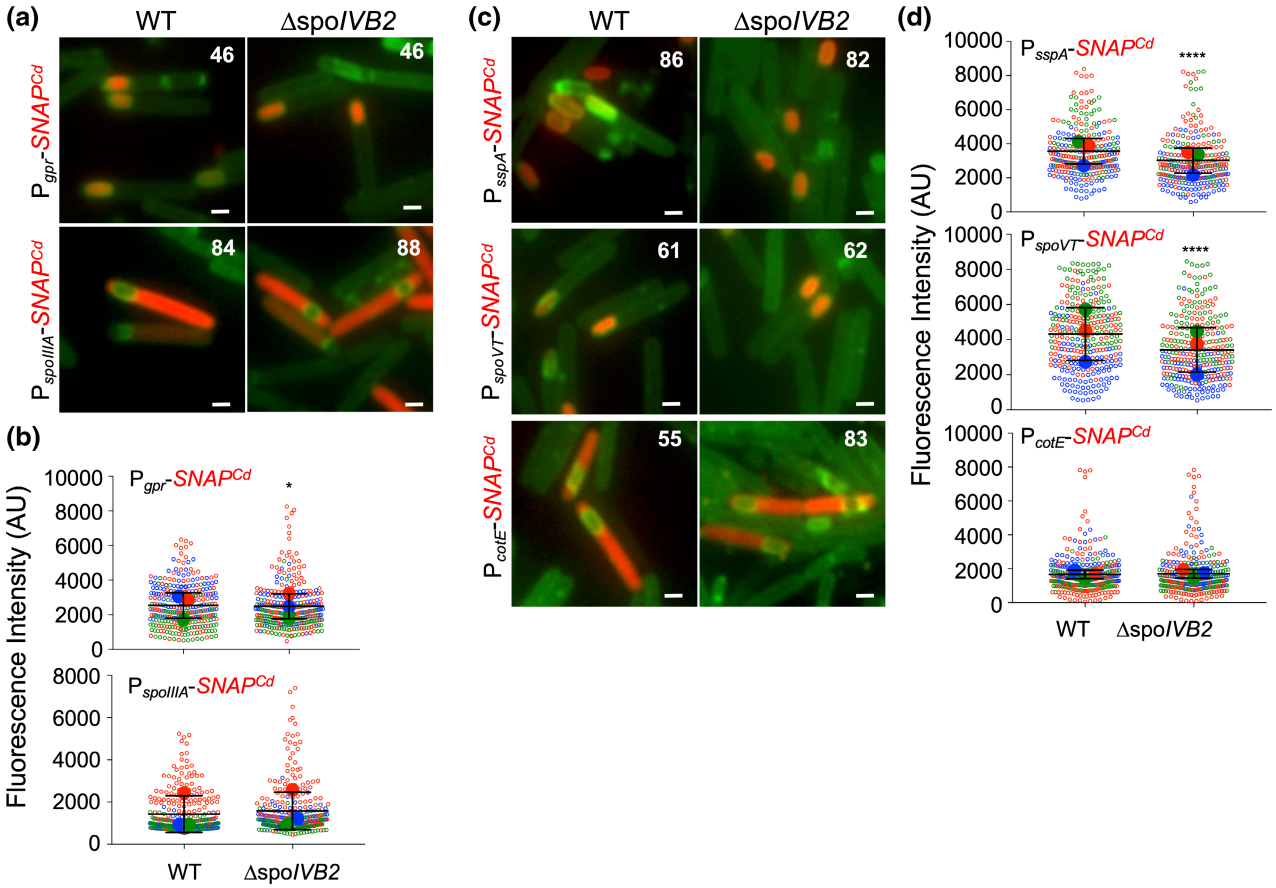


**FIGURE 4** Late forespore gene expression is impaired in the *spoIVB2* mutant. (a and c) Microscopy analysis of strains carrying transcriptional fusions of the *gpr*, *spoIIIA*, *sspA*, *spoVT*, and *cotE* promotors to the SNAP reporter in the WT and in the *spoIVB2* mutant. Cells were collected after 14 h of incubation in a 70:30 sporulation medium, stained with TMR-Star and the membrane dye MTG, and examined by fluorescence microscopy to monitor SNAP production. The merged image shows the overlap between the TMR-Star (red) and MTG (green) channels. The images are representative of the expression patterns observed. The numbers refer to the percentage of cells showing SNAP fluorescence. The data shown are from a representative experiment of at least three independent experiments. Scale bar, 1 μm. (b and d) Quantitative analysis of the fluorescence intensity in individual cells (in arbitrary units, AU) of the reporter strains for *gpr*, *spoIIIA*, *sspA*, *spoVT*, and *cotE* transcription, as indicated. SuperPlots were used to represent the data from three biological replicates; each dot corresponds to one cell, color-coded by experiment. The large circles represent the means from each experiment which were used to calculate the mean and standard error of the mean (horizontal lines) for the ensemble of the three experiments. The nonparametric Kolmogorov–Smirnov test (KS test) was applied to compare the combined distributions obtained from the 3 replicates (*$p < 0.01$; ****$p < 0.00001$). The *t*-test was also performed on the means with $p < 0.05$ for WT vs. Δ*spoIVB2* containing the *sspA*, and *spoVT* promotors fusion to the SNAP reporter.

cortex (Pereira et al., 2013). Significantly, the double *sspA*/*sspB* mutant also produces phase dark spores (Nerber & Sorg, 2021). Unfortunately, the expression of *sspB* was not detected using the $SNAP^{Cd}$ reporter. To test whether the impact on *sspA* expression in the *spoIVB2* mutant could be due to loss of *spoVT* expression, we monitored the expression of a $P_{spoVT}$-$SNAP^{Cd}$ transcriptional fusion in the mutant (Figure 4c,d). We found that, although the percentage of cells expressing $P_{spoVT}$-$SNAP^{Cd}$ is similar in the *spoIVB2* mutant and in the WT, the intensity of the fluorescence signal per cell in the mutant is decreased relative to the WT (Figure 4c,d). This decrease in *spoVT* expression may explain the effect observed on the expression of *sspA*. Another consequence of the reduced expression of *spoVT* observed in the *spoIVB2* mutant could also be the increased $P_{gpr}$-$SNAP^{Cd}$ expression, since in *C. difficile* SpoVT plays a role in the negative control of some $\sigma^F$ targets, including *gpr* (Pereira et al., 2013). In any case, it seems unlikely that the phenotype of the *spoIVB2* mutant results from the relatively minor alterations described in forespore-specific gene expression.

## 2.4 | *spoIVB2* is required for cleavage of the SpoIIP amidase/endopeptidase

In addition to its role in $\sigma^K$ signaling and cortex formation in *B. subtilis*, SpoIVB also cleaves SpoIIQ, a forespore membrane protein (Chiba et al., 2007; Jiang et al., 2005). In *C. difficile*, SpoIIQ was shown to be essential for engulfment and it interacts with SpoIIIAH, a mother cell membrane protein, with which it forms a transmembrane complex required for late transcription in both the forespore and the mother cell (Fimlaid et al., 2015; Serrano, Crawshaw, et al., 2016). The

SpoIIQ–SpoIIIAH complex (Q:H) also acts as an anchor for two PG hydrolases, SpoIID and SpoIIP (Dembek et al., 2018; Ribis et al., 2018), forming the engulfasome machinery required for forespore engulfment (Kelly & Salgado, 2019). SpoIID is produced under $\sigma^E$ control in the mother cell, whereas SpoIIP is produced in the forespore under $\sigma^F$ control (Ribis et al., 2018). In *B. subtilis*, SpoIIP is mainly produced in the mother cell and a third mother cell protein, SpoIIM, serves as a platform to bring together SpoIID and SpoIIP (Khanna et al., 2020). Although conserved in *C. difficile*, *spoIIM* is dispensable for sporulation in this organism (Dembek et al., 2018; Ribis et al., 2018).

In *C. difficile*, no cleavage of SpoIIQ is detected during sporulation (Ribis et al., 2018). In contrast, SpoIIP from *C. difficile* accumulates as four isoforms (Ribis et al., 2018). The predicted molecular weight (MW) of SpoIIP is 38 kDa, and that of SpoIIP lacking its signal peptide is 35 kDa ($SpoIIP_m$). In addition to cleavage of the signal peptide, SpoIIP is further processed into a form of about 34 kDa ($SpoIIP_t$) and one of approximately 25 kDa ($SpoIIP_c$). To test whether accumulation of $SpoIIP_t$ or $SpoIIP_c$ isoforms required SpoIVB2, the levels of SpoIIP in whole cell lysates prepared from WT, *spoIVB2* mutant, and complementation strains induced to sporulate on sporulation medium, were analyzed by immunoblotting. In the WT and complemented strains, SpoIIP starts to accumulate after 10 h of growth, $SpoIIP_t$ is first detected at hour 12 and $SpoIIP_c$ only after 14 h (Figure 5a). In the *spoIVB2* mutant, accumulation of SpoIIP and $SpoIIP_t$ follows the same pattern, but $SpoIIP_c$ is not detected, even at hour 24 (Figure 5). The four isoforms were detected in a *spoIVB1* mutant (Figure 5b), but $SpoIIP_c$ was not found in the *spoIVB1/spoIVB2* double mutant. As expected, if SpoIVB2 is involved in SpoIIP cleavage, increased accumulation of SpoIIP and $SpoIIP_t$ is observed in the *spoIVB2* and *spoIVB1/spoIVB2* double mutants at hour 24 of growth (Figure 5b).

$SpoIIP_c$ is also not detected in Δ*spoIIQ* and Δ*spoIID* mutants (Ribis et al., 2018). To test whether the absence of $SpoIIP_c$ resulted

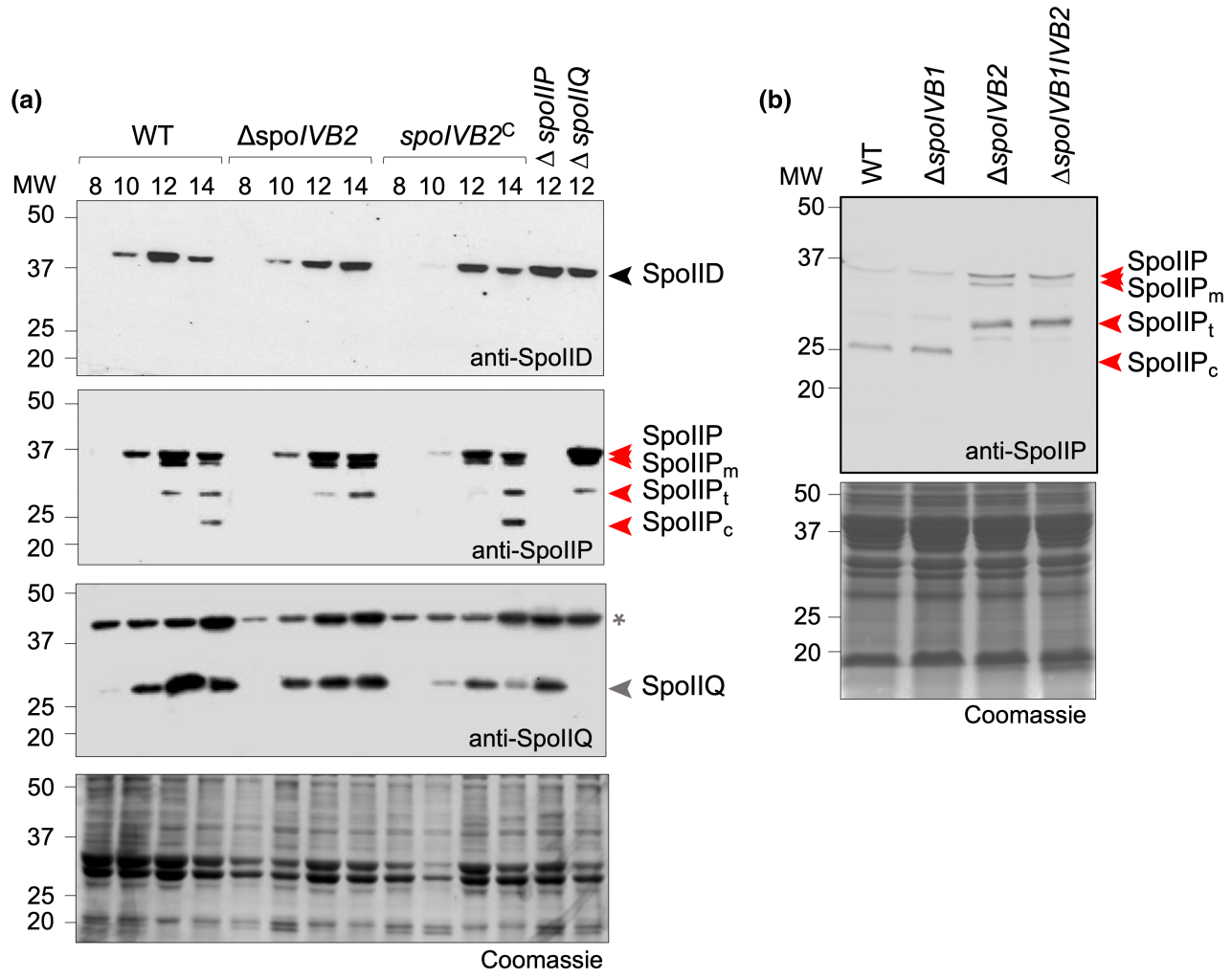


**FIGURE 5** SpoIIP cleavage depends on SpoIVB2. Immunoblot analyses of SpoIID, SpoIIP, and SpoIIQ in the indicated strains. The cells were collected at the indicated times (in hours, panel a) or after 24 h of incubation in a 70:30 sporulation medium (b). Extracts were prepared and proteins were subjected to immunoblotting using anti-SpoIID, anti-SpoIIP, and anti-SpoIIQ antibodies. The position of molecular weight markers (in kDa) is indicated on the left side of the panels; arrowheads on the right indicate the position of SpoIID (black), SpoIIP (red), and SpoIIQ (gray). Four forms of SpoIIP were detected: full-length (SpoIIP), mature, after cleavage of the signal peptide (SpoIIPm), truncated SpoIIP ($SpoIIP_t$), and cleaved ($SpoIIP_c$). The asterisk (*) denotes a cross-reacting protein recognized by the polyclonal anti-SpoIIQ antibody.

from altered levels of SpoIID or SpoIIQ, we used immunoblotting to monitor the accumulation of both proteins during sporulation. We found that the two proteins accumulate to similar levels in both the WT and the *spoIVB2* mutant (Figure 5a). Together, the results suggest a role for SpoIVB2 in SpoIIP proteolysis.

We also tested whether SpoIVB cleaved SpoIIP in *B. subtilis*. We used immunoblotting to monitor the accumulation of SpoIIP in whole cell lysates prepared from the WT and a *spoIVB* mutant induced to sporulate in Difco sporulation medium (DSM). We found no evidence for cleavage of *B. subtilis* SpoIIP during sporulation (Figure S3).

## 2.5 | SpoIVB2 cleaves SpoIIP in vitro

To test if SpoIVB2 directly cleaved SpoIIP, SpoIVB1, SpoIVB2, and SpoIIP were recombinantly expressed in *Escherichia coli* and purified by affinity chromatography followed by size exclusion chromatography to remove any potential *E. coli* contaminants (Figure 6a, first three lanes in the Coomassie-stained SDS–PAGE). The three proteins were produced without their transmembrane domains. The proteins were incubated at 37°C in the presence of SpoIVB2 or SpoIVB1. While the size of SpoIIP$^{\Delta SP}$ is 43 kDa, when incubated with SpoIVB2, a new cleavage product of SpoIIP (SpoIIP*), migrating at approximately 20 kDa, along with smaller-sized bands, accumulated (Figure 6a). This coincided with a reduction in the level of SpoIIP$^{\Delta SP}$ (Figure 6a). In contrast, SpoIVB1 was unable to cleave SpoIIP, consistent with its inability to replace SpoIVB2 for SpoIIP cleavage (Figure 6).

To further confirm that the cleavage of SpoIIP was dependent on SpoIVB2, a catalytic inactive protease (SpoIVB2$^{S301A}$) was incubated with SpoIIP. In our assays, SpoIVB2 consistently accumulated at a lower level than the inactive SpoIVB2$^{S301A}$, possibly due to its autoproteolytic activity, as observed in *B. subtilis* (Wakeley et al., 2000). In any case, SpoIIP was still cleaved by SpoIVB2, but not by the catalytically inactive SpoIVB2$^{S301A}$ variant (Figure 6b).

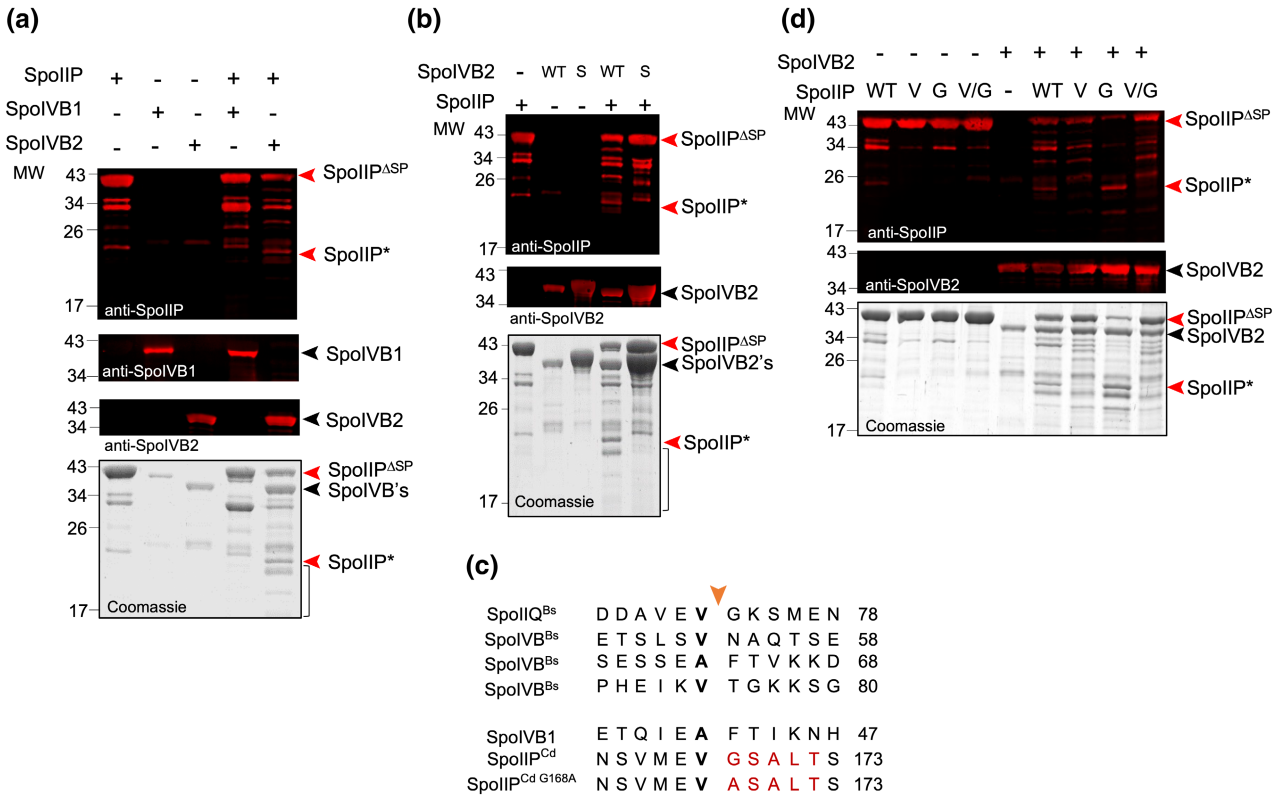


**FIGURE 6** Identification of the SpoIVB2 cleavage site in SpoIIP. (a and b) Cleavage assay with recombinantly expressed SpoIIP and SpoIVB2 variants shows that SpoIVB2 cleaves SpoIIP in vitro. (a) Only catalytically active SpoIVB2 can cleave SpoIIP when 40 μg of recombinant proteins were incubated in the indicated combinations. (b) Purified SpoIVB2 (WT) or SpoIVB2$^{S301A}$ (S) were incubated with purified SpoIIP. Note that the same concentration of SpoIVB2 and SpoIVB2$^{S301A}$ was used in the incubation and loaded on the gel (4 μg). (c) Alignment of the SpoIVB-dependent cleavage sites in SpoIIQ and SpoIVB of *Bacillus subtilis*, and the putative SpoIVB-dependent cleavage sites in *Clostridioides difficile* SpoIVB1 and SpoIIP. The orange arrowhead indicates the cleavage site. Residues in red were obtained by Edman sequencing analysis for the SpoIIP* variant. (d) Cleavage assay with recombinantly expressed SpoIIP variants (WT, SpoIIP$^{\Delta SP}$; V, SpoIIP$^{V167L}$; G, SpoIIP$^{G168A}$, and V/G, SpoIIP$^{V167L/G168A}$) and SpoIVB2. For panels a, b, and d: All samples were analyzed by 15% SDS–PAGE. Gels were stained with Coomassie or subject to immunoblotting with anti-SpoIIP, anti-SpoIVB1, and anti-SpoIVB2 antibodies. The position of MW markers (in kDa) is indicated on the left side of the panels; arrowheads on the right indicate the position of SpoIIP (red) and SpoIVB proteins (black). Several forms of SpoIIP were detected: full-length SpoIIP$^{\Delta SP}$ (around 43 kDa), and likely proteolytic products that accumulate independently of the presence of SpoIVB1 and SpoIVB2 and a product, SPoIIP*, whose accumulation depends on the presence of SpoIVB2. Brackets in panels a and b represent proteolytic products that are detected after SpoIIP cleavage by SpoIVB2.

## 2.6 | Identification of the SpoIIP cleavage site

From the cleavage assay in Figure 6b, the N-terminal sequence of SpoIIP* was determined by Edman degradation as "GSALT," where "G" corresponds to glycine 168 of SpoIIP (Figure 6c). SpoIIP variants with substitutions of glycine 168 to alanine or valine 167 to leucine, or both, were produced. SpoIIP$^{V167L}$ and SpoIIP$^{V167L/G168A}$ proteins were not cleaved by SpoIVB2 (Figure 6d). However, SpoIVB2 cleaved SpoIIP$^{G168A}$ at alanine 168 as verified by N-terminal sequencing (Figure 6c,d).

Alignment of previously characterized SpoIVB$^{Bs}$ cleavage sites identified in SpoIIQ$^{Bs}$ and SpoIVB$^{Bs}$ shows that SpoIVB$^{Bs}$ cleaves after either alanine or valine, with no primary sequence conservancy in the adjacent residues (Figure 6c). Although in vitro, the substitution of valine at the cleavage site by other amino acids renders SpoIIQ$^{Bs}$ resistant to SpoIVB, only the substitution to methionine was shown to prevent cleavage both in vivo and in vitro (Chiba et al., 2007). Therefore, we complemented a Δ*spoIIP* mutant with a plasmid-bearing WT *spoIIP* (strain *spoIIP*$^{C}$) and a *spoIIP*$^{V167M}$ allele under the $P_{tetA}$ control. We used immunoblotting to analyze SpoIIP levels in cell lysates prepared from the *spoIIP*$^{C}$ and *spoIIP*$^{V167M}$ strains, induced on sporulation medium supplemented with anhydrotetracycline (ATc) after 10 h of growth. The four isoforms of SpoIIP were detected in the *spoIIP*$^{C}$ strain but SpoIIP$_c$ was not detected in the *spoIIP*$^{V167M}$ strain (Figure 7a). Cleavage at Val167 results in a fragment of approximately 19.4 kDa, which agrees with the resulting SpoIIP* in vitro cleavage product (~20 kDa) but not with the band that accumulates in *C. difficile* extracts, SpoIIP$_c$ (~25 kDa) (Figure 7a,b). The reason for the size discrepancy is presently unknown. In any case, Val167 has a crucial role in the SpoIVB2-dependent formation of SpoIIP$_c$.

## 2.7 | Cleavage of SpoIIP by SpoIVB2 abolishes the enzymatic activity

SpoIIP and SpoIID are PG hydrolases, part of the engulfasome machinery required for PG remodeling during engulfment. SpoIIP is an amidase, that removes the peptide stems from the glycan chains and an endopeptidase that cleaves the crosslinks between stem peptides. SpoIID is a lytic transglycosylase that acts on the products generated by SpoIIP (Dembek et al., 2018; Kelly & Salgado, 2019) (Figure 8a). To investigate whether cleavage of SpoIIP by SpoIVB2 affected enzymatic activity, purified mature SpoIIP, and SpoIIP* (SpoIIP$_{168–339}$) were incubated with PG purified from *E. coli*, followed by digestion with the muramidase cellosyl, and analysis of the PG fragments by liquid chromatography–mass spectrometry (LC–MS) (Dembek et al., 2018).

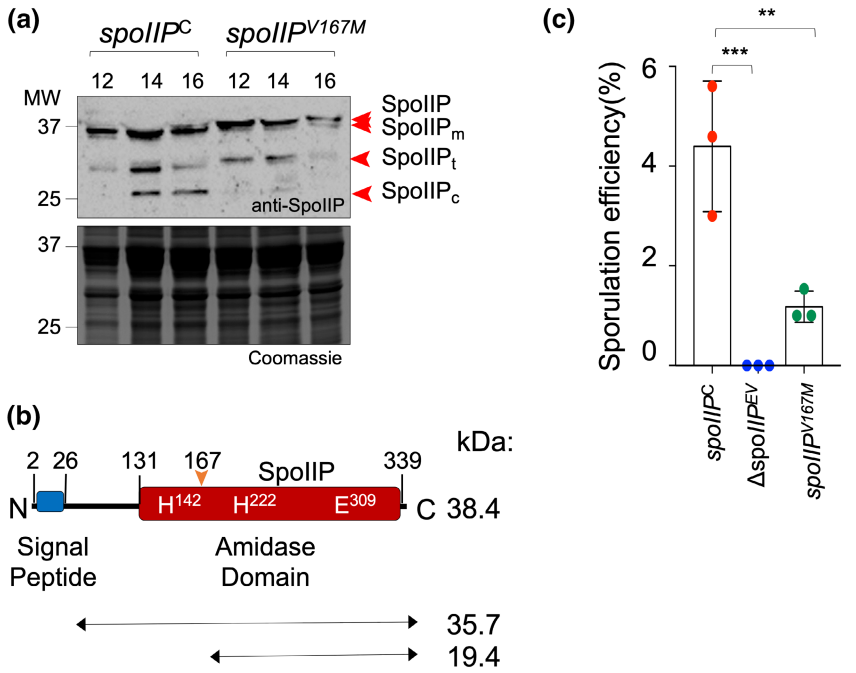


FIGURE 7 Cleavage of SpoIIP by SpoIVB2 is not essential for sporulation. (a) Immunoblot analysis of SpoIIP in the indicated strains. The cells were collected at the indicated times (in hours) of incubation in a 70:30 sporulation medium. The position of molecular weight markers (in kDa) is indicated on the left side of the panels, and the arrowheads on the right indicate the position of the four forms of SpoIIP. Note that in the *spoIIP*$^{V167M}$-bearing strain, the SpoIIP$_c$ form is not detected. The immunoblots shown are representative of the results of at least two independent experiments. (b) Schematic representation of SpoIIP: signal peptide, residues 2–26; amidase domain, residues 131–339. The proposed catalytic residues His142, His222, and Glu309 are represented and the SpoIVB-dependent cleavage site at amino acid 167 is indicated by an orange arrowhead. (c) Sporulation efficiency for the indicated strains, incubated for 24 h in a 70:30 sporulation medium. EV; empty vector. The results shown are averages and standard deviations for three biological replicates. Asterisks indicate statistical significance determined with a two-way ANOVA (**$p < 0.01$; ***$p < 0.001$).

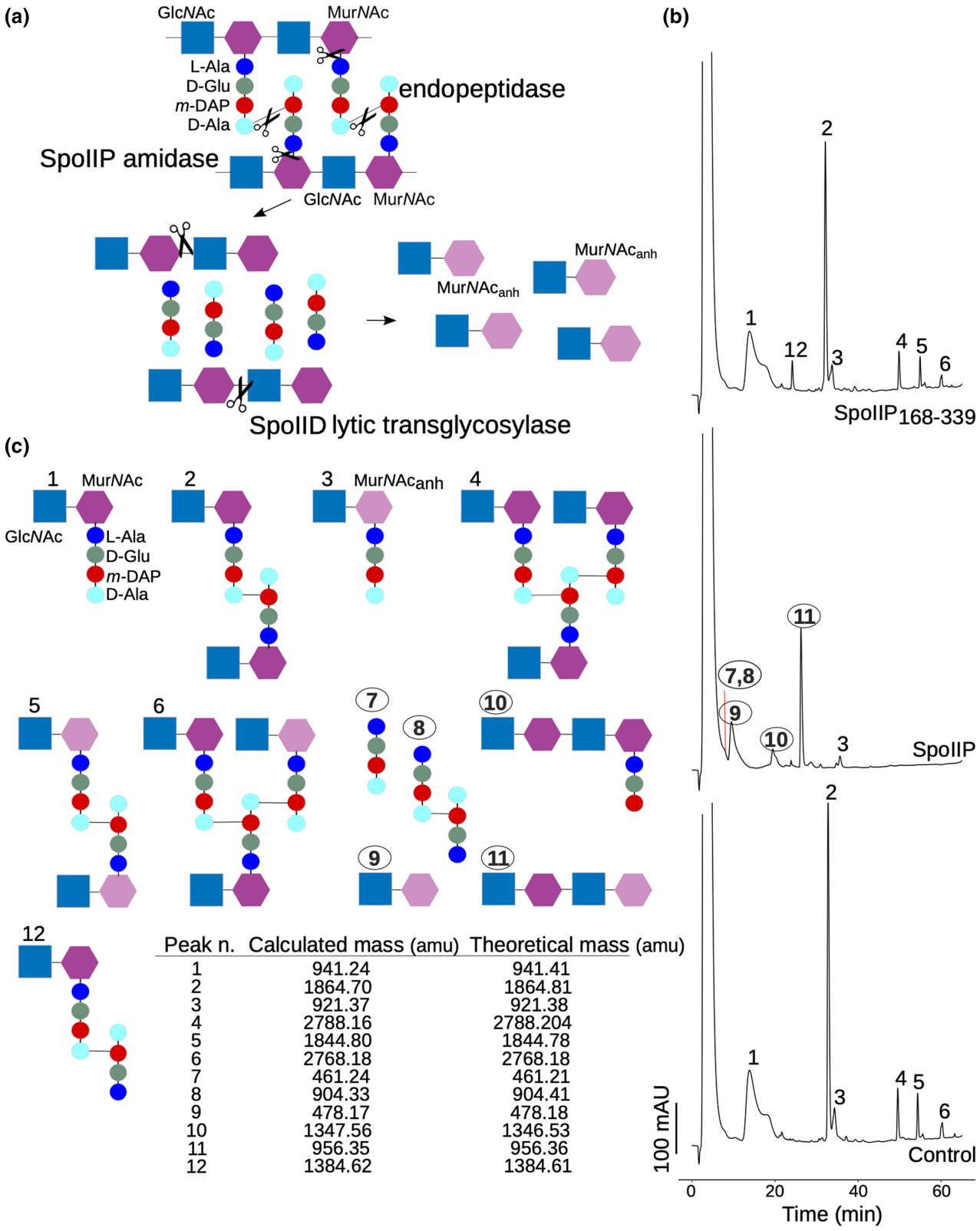


| Peak n. | Calculated mass (amu) | Theoretical mass (amu) |
|---|---|---|
| 1 | 941.24 | 941.41 |
| 2 | 1864.70 | 1864.81 |
| 3 | 921.37 | 921.38 |
| 4 | 2788.16 | 2788.204 |
| 5 | 1844.80 | 1844.78 |
| 6 | 2768.18 | 2768.18 |
| 7 | 461.24 | 461.21 |
| 8 | 904.33 | 904.41 |
| 9 | 478.17 | 478.18 |
| 10 | 1347.56 | 1346.53 |
| 11 | 956.35 | 956.36 |
| 12 | 1384.62 | 1384.61 |

As expected, SpoIIP showed amidase activity, hydrolyzing amide bonds between the glycan chain (MurNAc) and the peptide stems, to release crosslinked tetra-tetrapeptide dimers (Figure 8b,c, peak 8) and glycan chains, which were then digested by cellosyl into di- and tetrasaccharides (Figure 8b,c, peaks 9–11). The expected tetrapeptide monomers produced by endopeptidase activity were also identified as reaction products (Figure 8b,c, peak 7, Figure S4).

Cleavage by SpoIVB2 at position 167 removes H142, one of the three proposed catalytic residues (His142, His222, and Glu309) involved in amidase activity (Dembek et al., 2018) (Figure 7b) and we hypothesized this isoform would be inactive. Indeed, no significant

**FIGURE 8** Cleavage of SpoIIP by SpoIVB2 inactivates the enzyme. (a) Schematic representation of the sequential enzymatic activities of the SpoIID/P machinery, demonstrating how the smallest products of digestion are produced, based on in vitro assays using *Escherichia coli* PG as the substrate (Dembek et al., 2018). SpoIIP amidase activity produces denuded long glycan strands and cross-linked tetra-tetrapeptides, which are further processed into tetrapeptide monomers by the endopeptidase activity. SpoIID processes the denuded glycan strands to produce Glc*N*Ac-Mur*N*Ac$_{anh}$ disaccharides. Glc*N*Ac, *N*-acetyl*glucosamine* (blue square); Mur*N*Ac, *N*-acetylmuramic acid (purple hexagon); L-alanine (blue circles); D-glutamic acid (olive green circles); *meso*-2,6-diaminopimelic acid (*m*DAP, red circles); D-alanine (cyan circles); Mur*N*Ac$_{anh}$, anhydro *N*-acetylmuramic acid (pale purple hexagons). Black line indicates 4–3 cross-links between D-alanine and *m*DAP. (b) SpoIIP has both amidase and endopeptidase activity but both enzymatic activities are abolished in SpoIIP$_{168–339}$. Enzymatic activity was assayed by analyzing the products of PG digestion by the different proteins through LC–MS, as detailed in Materials and Methods and in the supplementary material. PG from *E. coli* BW25113Δ6LDT was digested overnight with SpoIIP or SpoIIP$_{168–339}$, before overnight digestion with cellosyl. In the control reaction, PG was digested only with cellosyl. The reaction products were separated and identified by LC–MS and numbered peaks of interest were identified by MS. Chromatograms represent, from bottom to top: control; SpoIIP and SpoIIP$_{168–339}$. (c) Proposed structures of muropeptides identified and numbered in the chromatograms in panel b. Theoretical neutral masses and the masses calculated from mass spectra are presented in the table.

differences in the muropeptide composition were observed between PG incubated with (inactive) SpoIIP$_{168–339}$ and the cellosyl-only digest (Figure 8b, top and bottom). The apparent enrichment of a disaccharide tetra-tetrapeptide dimer (Figure 8b,c, peak 12), was not statistically significant when quantifying the area under each curve (Figure S4).

Importantly, tetrapeptide monomers were absent, indicating that endopeptidase activity is also abolished in this isoform and that at least some of the yet to be identified endopeptidase catalytic residues are present in the N-terminal region.

Analysis of the AF2 predicted models for both forms suggests that cleavage at position 167 alters the secondary and tertiary structure of SpoIIP, with one β-strand deleted and subsequent disruption of the β-sheet containing the active site (Figure S5a,b). Importantly, Glu309, also proposed to be involved in amidase activity, is predicted to have a different orientation, forming new interactions with His222, which could enhance the disruption of catalytic activity caused by the lack of H142 (Figure S5c,d). It is also noteworthy that the cleavage removes a loop predicted to partially occlude the active site, exposing the catalytic residues, which might further affect enzymatic activity. Overall, cleavage of SpoIIP by SpoIVB2 produces a form of the protein, SpoIIP$_c$, with impaired activity and likely altered conformation. Since SpoIIP activity generates the products for SpoIID, we hypothesize that the cleavage of SpoIIP by SpoIVB2 may inactivate the engulfasome hydrolytic activity.

## 2.8 | SpoIIP cleavage is not required for sporulation or germination

To determine whether SpoIIP cleavage was essential for sporulation, we measured the titer of heat-resistant spores formed by strains Δ*spoIIP*, *spoIIP*$^C$, and *spoIIP*$^{V167M}$, incubated on sporulation medium for 24 h. The formation of heat-resistant spores was restored in the *spoIIP*$^C$ strain, complementing the asporogeneous phenotype of the Δ*spoIIP* mutant (Figure 7c). Strain *spoIIP*$^{V167M}$ produced about 25% of the heat-resistant spores produced by *spoIIP*$^C$ (Figure 7c). Nevertheless, microscopic observation of the *spoIIP*$^{V167M}$ strain after 24 h of incubation on sporulation medium did not reveal a clear block at any stage of sporulation, and released phase bright spores were easily seen (12%–13% of the sporulating cells in both strains).

To test if the reduced resistance to heat observed in the *spoIIP*$^{V167M}$ strain was due to impaired germination, we tested the germination efficiency of spores purified from *spoIIP*$^C$ and *spoIIP*$^{V167M}$ in response to taurocholate (TA) (see the Supplementary Materials and Methods). No differences were detected in the kinetics or efficiency of germination between the two strains (Figure S7). This is reminiscent of the situation in *B. subtilis* where the cleavage of SpoIIQ by SpoIVB is not needed for the production of heat-resistant spores (Chiba et al., 2007).

## 3 | DISCUSSION

A SpoIVB-type protease is part of a genomic signature for sporulation (Abecasis et al., 2013; Browne et al., 2016). In *C. difficile*, this signature protease is the product of *spoIVB2* because this gene, and not its paralog, *spoIVB1*, is essential for sporulation. Although SpoIVB1 and SpoIVB2 share close to 31% of sequence identity for 94% of the aligned amino acid residues, we show that SpoIVB1 is unable to replace SpoIVB2 during sporulation. Differences in the time of gene expression are not sufficient to explain this phenotype since the expression of *spoIVB1* from the *spoIVB2* promotor did not restore sporulation to the *spoIVB2* mutant. SpoIVB1 is also not able to cleave at least one of the SpoIVB2 substrates, SpoIIP (Figure 6a). Substrate specificity is likely mediated by the PDZ domain present in both SpoIVB1 and SpoIVB2 (Figure 1b,c). PDZ domains are involved in protein–protein interactions and, in SpoIVB$^{Bs}$, this domain is required for self-recognition leading to trans-self-cleavage and also for the interaction with BofA (Dong & Cutting, 2004; Hoa et al., 2001; Muley et al., 2019). While SpoIVB1 may have sporulation-specific substrates, their cleavage is not essential for the production of heat-resistant spores.

PDZ domains also have regulatory roles in secreted serine proteases such as CtpB from *B. subtilis* and Prc from *E. coli*. CtpB cleaves SpoIVFA, after a first cleavage by SpoIVB, and is thus involved in $\sigma^K$ activation during sporulation (Campo & Rudner, 2006; Pan et al., 2003; Zhou & Kroos, 2005). In CtpB, the PDZ domain blocks access to the active site (Mastny et al., 2013). In Prc, the catalytic site is in a default misaligned conformation that maintains the protease inactive (Chueh et al., 2019). The binding of a substrate to the PDZ domain triggers a structural rearrangement that is communicated to

the active site and renders it competent for catalysis. Since the proposed catalytic triad also appears misaligned in the AF2 predicted structures of the SpoIVB proteins (Figure 1b), the active site may similarly be formed after binding of a substrate to the PDZ domain.

We show that the *spoIVB2* mutant is blocked after engulfment completion, accumulating free immature "sporelets" and sporangia of immature forespores that lack the cortex (Figure 2). The catalytic activity of SpoIVB2 is required for cortex formation since the phenotype of the Δ*spoIVB2* mutant is not complemented by an allele encoding a catalytic inactive protease (Figure 2a). The Δ*spoIVB2* mutant also shows deposition of some coat/exosporium material and consistently, shows activity of $\sigma^K$ (Figure 2) (Pereira et al., 2013). In contrast, we found that deletion of *spoIVB2* had a negative impact on late, $\sigma^G$-dependent gene expression in the forespore, as *sspA* and *spoVT* transcription was slightly reduced (Figure 4). *sspA*, as *sspB*, are under the dual control of $\sigma^G$ and SpoVT and both code for small acid-soluble proteins, required to protect spores from damage caused by UV radiation (Nerber & Sorg, 2021; Saujet et al., 2013). Recent work, however, has shown that an Δ*sspA*/*sspB* mutant produces phase dark spores (Nerber & Sorg, 2021) and importantly, mutations in *spoIVB2* suppressed the defect in sporulation of the double mutant (Nerber et al., 2023). Since mutations that suppressed the phenotype of the Δ*sspA*/*sspB* double mutant also mapped to *sigG* and *spoVT*, SspA/SspB could be directly involved in the control of forespore gene expression, including *spoIVB2* (Nerber et al., 2023). Because *spoIVB2* is required for proper transcription of at least *sspA* and *spoVT* (Figure 4) we propose that a negative feedback loop is established that may adjust the levels of SpoIVB2 and SspA/SspB (Figure 9a,b). This regulatory function may be independent of the proteolytic activity of SpoIVB2 required for cortex synthesis, as its catalytic domain resides in the

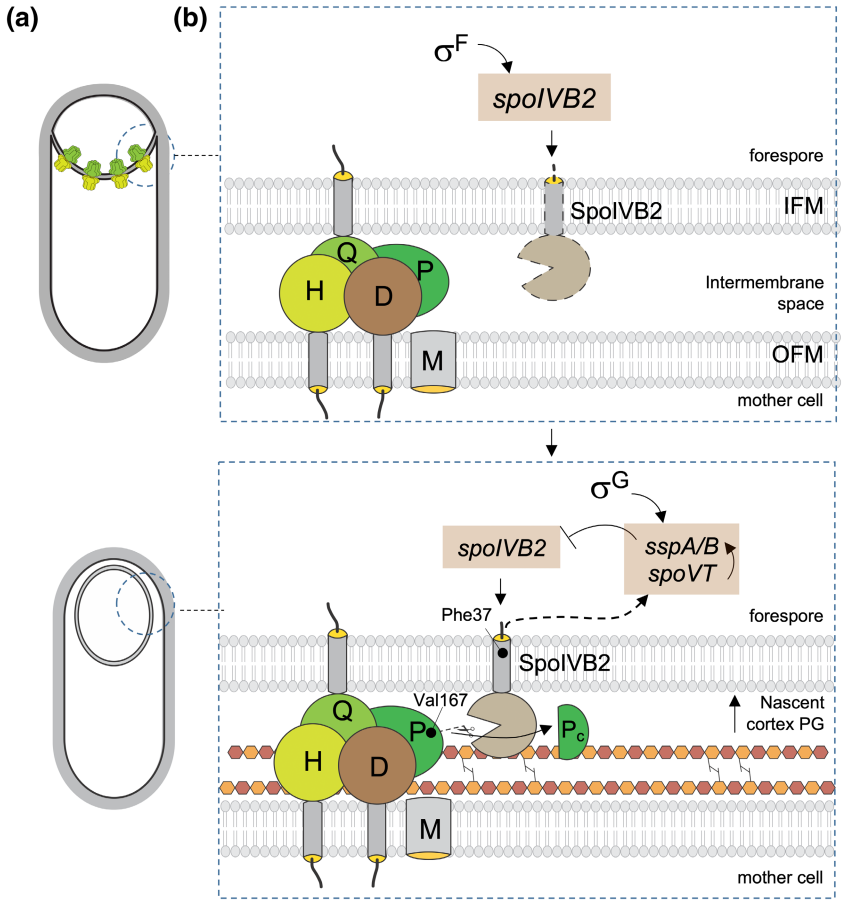


**FIGURE 9** Model for the cleavage of SpoIIP by SpoIVB2 during sporulation in *Clostridioides difficile*. (a) Diagram of sporulating cells during and following engulfment completion. The SpoIIIAH (light green) and SpoIIQ proteins (darker green), only present during engulfment, are thought to have a zipper-like function and to be part of a channel complex through which the mother cell maintains metabolic potential in the forespore. (b) The engulfasome complex, consisting of SpoIIQ (Q), SpoIIIAH (H), SpoIID (D), and SpoIIP (P). SpoIIM (M), although not required for sporulation, is also represented. SpoIVB2 is produced in the forespore under the control of $\sigma^F$ but is thought to be kept at low levels during engulfment (dashed lines). The protein is translocated to the intermembrane space, where it remains associated with the inner forespore membrane (IFM). Soon after engulfment completion, SpoIVB2 cleaves SpoIIP at residue V167, to generate the SpoIIP$_c$ form (P$_c$). The function of SpoIVB2 is somehow required for the synthesis of the cortex PG layer which takes place across the outer forespore membrane (OFM). The model predicts that *sspA*/*sspB*, which are under the control of $\sigma^G$, repress transcription of *spoIVB2*, which in turn is somehow required for *sspA*/*sspB* and *spoVT* expression. The negative feedback loop thus established may limit the levels of SspA/B and SpoIVB2. The GCW is not represented for simplicity. None of the molecules represented are to scale.

intermembrane space; it may require the 24 amino acids at the N-terminal of the protein, thought to localize in the forespore cytoplasm (Figure 1c). In agreement with this hypothesis, suppressors of the defect of the *sspA/sspB* double mutant were a synonymous mutation in codon 37 of *spoIVB2*, which specifies a phenylalanine located in the transmembrane helix, and a missense mutation at codon 20 leading to an alanine to threonine substitution (Nerber et al., 2023).

Here, we also demonstrate that SpoIIP is cleaved late during sporulation in a SpoIVB2-dependent manner to produce $SpoIIP_c$ (Figure 5). We show that SpoIVB2 directly cleaves SpoIIP at Val167 and that substitutions V167L or V167M prevent cleavage (Chiba et al., 2007) (Figures 6 and 7). Since $SpoIIP_{168-339}$, corresponding to $SpoIIP_c$ has no detectable amidase or endopeptidase activities, we suggest that SpoIIP is inactivated after engulfment completion when this activity is no longer needed (Figure 8). The cortex is essential for the reduction of the water content of the spore core, which in turn determines resistance to heat (Setlow & Christie, 2023). The maintenance of an active SpoIIP may give rise to spores with an altered cortex, explaining the observed 75% reduction in spore heat resistance in the V167M mutant (Figure 7). Since this phenotype is more subtle than the sporulation phenotype found for the *spoIVB2* null mutant, it seems likely that SpoIVB2 has substrates other than SpoIIP that play a role in cortex synthesis.

In *B. subtilis*, $SpoIVB^{Bs}$ appears to be maintained at low levels during engulfment but stabilized once engulfment is completed (Doan & Rudner, 2007). As a result, $SpoIVB^{Bs}$ substrates, such as SpoIIQ and SpoIVFA, are only cleaved after engulfment completion. This degradative pathway is part of the $\sigma^K$ checkpoint which ensures that the sigma factor does not become active before engulfment completion. Considering that accumulation of $SpoIIP_c$ is only detected late (Figure 5) and not at all in engulfment defective mutants such as Δ*spoIID* and Δ*spoIIQ* (Figure 5; 40), SpoIVB2 may also be degraded during engulfment in *C. difficile*. Therefore, SpoIVB2 accumulation and/or activity may also be coupled to engulfment completion in *C. difficile* (Figure 9).

We do not yet know how SpoIVB2 signals cortex synthesis by the mother cell. Synthesis of PG in the periplasmic space of Gram-negative bacteria bears some parallel with the synthesis of the GCW and cortex in the intermembrane space (Pazos et al., 2017). Growth of the PG requires the action of hydrolases that cleave the cross-links for the insertion of new material. These two antagonist activities of hydrolases and synthetases of PG must be somehow regulated. In *E. coli*, Prc (see above) regulates both the PG hydrolase MepS and the penicillin-binding protein 3 (PBP3) by proteolysis (Hara et al., 1991; Singh et al., 2015). Similarly, one possibility is that SpoIVB2 also regulates the activity of one or more PG synthases. We screened for mutants that would bypass the need for *spoIVB2* for the formation of heat-resistant spores, but none were identified. Several redundant mechanisms are possibly involved in the activation of cortex synthesis; it is also possible that the genes involved are essential for viability or sporulation or that SpoIVB2 has multiple substrates.

In any event, the SpoIVB2-dependent proteolysis of SpoIIP, which we describe, may lead to a rearrangement of the engulfasome following engulfment completion, when the cortex starts to be synthesized in the intermembrane space. We do not presently know whether the engulfasome is inactivated following engulfment completion in *B. subtilis*, but we note that there are differences in the process between the two organisms. For instance, unlike in *B. subtilis*, *spoIIM* is not required for engulfment *in C. difficile*, *spoIIP* is produced exclusively in the forespore and carries a signal peptide, and the SpoIIQ–SpoIIIAH and SpoIID–SpoIIP complexes are at least partially redundant (Kelly & Salgado, 2019; Khanna et al., 2020). As SpoIVB2 also impacts late gene expression in the forespore, the protein may have a role in coordinating both morphogenesis and gene expression at a late stage in development. The identification of the molecular basis for the *spoIVB2* mutant phenotype remains a main challenge for future research. Since many serine proteases play essential roles in disease development, they have been considered as druggable targets (Harish & Uppuluri, 2018). Inhibitors of SpoIVB2, which is largely confined to spore-forming bacteria, could prevent the formation of spores, and in this way halt the persistence and transmission of this enteric pathogen.

## 4 | MATERIALS AND METHODS

### 4.1 | Bacterial strains, media, and general methods

Bacterial strains and their relevant properties are listed in Table S1. Routine growth of *E. coli*, *B. subtilis*, and *C. difficile* strains was as previously described (Abecasis et al., 2013; Martins et al., 2021). For the induction of sporulation in *C. difficile*, strains were grown on 70:30 agar medium as described before (Putnam et al., 2013). Sporulation in *B. subtilis* was induced in DSM (Abecasis et al., 2013). Sporulation efficiency was determined as previously described (Martins et al., 2021). All the plasmids and primers used in this work are listed in Tables S2 and S3, respectively.

### 4.2 | Construction of the *spoIVB1* and *spoIVB2* mutants

Plasmids pDM26 and pAF2 were used to generate in-frame deletions of the *spoIVB1* and *spoIVB2* genes in *C. dificile* 630Δ*erm*Δ*pyrE* by allelic exchange (Ng et al., 2013). The mutations were confirmed by PCR using primers spoIVB1_D and spoIVB1_R for spoIVB1, and spoIVB2_D and spoIVB2_R for spoIVB2 (Figure S1). The restoration of *pyrE* was done using pMTL-YN1C and confirmed by PCR using primers pyrE_D and pyrE_R (Figure S1).

### 4.3 | SNAP labeling, fluorescence microscopy, and image analysis

Samples of sporulating cultures were labeled with the membrane dye Mitotracker™ Green FM (MTG, Molecular Probes) and,

when indicated, also with TMR-Star, and imaged as described (Martins et al., 2021). Images were acquired and analyzed using the Metamorph software suite (Molecular Devices) and adjusted and cropped using Photoshop S4. Statistical analysis was carried out using GraphPad Prism 7.0a (GraphPad Software Inc.). The data from three independent experiments were represented using SuperPlots.

### 4.4 | Transmission electron microscopy

For thin sectioning TEM analysis, sporulating cells were processed as described previously (Henriques et al., 1998) and imaged on a Hitachi H-7650 Microscope equipped with an AMT digital camera operated at 120 keV.

### 4.5 | Preparation of cell extracts and immunoblotting

Whole-cell extracts were obtained as described previously (Martins et al., 2021). Proteins (10 μg) were resolved by SDS–PAGE (12%) and subject to immunoblotting with anti-SpoIIP (*C. difficile* 1:5000; affinity pure anti-SpoIIP *B. subtilis* 1:30,000), anti-SpoIIQ (1:5000), anti-SpoIID (1:5000), SpoIVB1 (1:5000), and SpoIVB2 (1:2500). An anti-rabbit secondary antibody conjugated to horseradish peroxidase (1:5000; Sigma) was used and the immunoblots were developed with enhanced chemiluminescence reagents (Amersham Pharmacia Biotech). When goat anti-rabbit IRDye 680RD (1:20,000; LI-COR Biosciences) was used, the membrane was imaged with a LI-COR Odyssey M using the 700 nm channel. Images were adjusted and cropped using ImageJ (http://rsbweb.nih.gov/ij/).

### 4.6 | AlphaFold2 modeling

AlphaFold2 (AF2, Jumper et al., 2021) models were generated in the open-access AlphaFold Colab notebook (https://colab.research.google.com/github/deepmind/alphafold/blob/main/notebooks/AlphaFold.ipynb) using the sequences of the relevant proteins or isoforms as input, with all other default parameters. The highest-ranking model after each prediction was analyzed and superimposed in Coot (Emsley & Cowtan, 2004) or Pymol Molecular Graphics System (Schrödinger, LLC). Structural representations were generated using PyMOL.

### 4.7 | SpoIIP, SpoIVB1, and SpoIVB2 recombinant expression and purification

SpoIVB's proteins were produced without the transmembrane domain and SpoIIP without the signal peptide. Plasmids pHN141 (SpoIVB2), pHN148 (SpoIVB2$^{S301A}$), pHN175 (SpoIIP), pHN193 (SpoIVB1), pHN275 (SpoIIP$^{V167L}$), pHN276 (SpoIIP$^{G168A}$), and pHN277 (SpoIIP$^{V167L/G168A}$) were transformed into *E. coli* Rosetta. The proteins were overproduced and purified as detailed in the supplementary information.

### 4.8 | Cleavage assays

A quantity of 40 μg of purified SpoIVB1, SpoIVB2, and SpoIIP was added into buffer A (300 mM NaCl, 500 μM $ZnCl_2$, 50 mM Tris–HCl, pH 7.5) for 1 h at 37°C. For SpoIVB2 *and* SpoIVB2$^{S301A}$ variants, 40 μg of purified protein were incubated with 40 μg of SpoIIP into buffer A for 2 h at 37°C in various combinations. For SpoIIP variants, 40 μg of protein and/or 40 μg of purified SpoIVB2 were incubated in buffer A for 2 h at 37°C. All samples were boiled with Laemmli sample buffer and analyzed by 15% SDS–PAGE.

### 4.9 | Peptidoglycan isolation, digestion, and mass spectrometry analysis

SpoIIP$_{27–339}$, equivalent to the SpoIIP$^{m}$, used in the PG assays was purified as described previously (Dembek et al., 2018). Plasmid pCGR002 (TEV-cleavable 6xHis tag SpoIIP$_{168–339}$; Table S2) was transformed into *E. coli* Lemo21 (DE3) (NEB) and the protein was purified from inclusion bodies, as detailed in supplementary information. Circular dichroism analysis of SpoIIP$_{168–339}$ (Figure S6) was carried out as detailed in the supplementary information to confirm correct protein folding. Isolation of PG from *E. coli* BW25113Δ6LDT (Kuru et al., 2017), lacking all 6 YkuD family proteins (LD-transpeptidases and PG-Lpp amidase), was carried out as previously described for analysis of SpoIIP and SpoIID activity (Dembek et al., 2018). Digestion reactions were prepared as previously described (Dembek et al., 2018) with an extra step, where 0.07 mg mL$^{-1}$ of cellosyl were added for a further 24 h incubation. Reactions were terminated by boiling and samples were dried (ScanVac), dissolved in 0.25 M ammonium hydroxide pH 9.0, and reduced with ~1 mg of tetramethylammonium borohydride. After 30 min, the reduction was terminated by adjusting the pH 3–4 with 20% HPLC-grade formic acid. LC–MS/MS analysis was carried out in an 1100 HPLC system (Agilent, UK) at 35°C with a step gradient between 0.1% (v/v) water/formic acid and 0.1% (v/v) acetonitrile/formic acid and the eluate was directed to the mass spectrometer (LTQ Ion Trap MS, Thermo) via an IonMax™ electrospray ion source (Thermo), as detailed in the supplementary information.

## AUTHOR CONTRIBUTIONS

**Diogo Martins:** Investigation; writing – original draft; writing – review and editing. **Hailee N. Nerber:** Investigation; writing – original draft. **Charlotte G. Roughton:** Investigation; writing – original draft. **Amaury Fasquelle:** Investigation. **Anna Barwinska-Sendra:** Supervision. **Daniela Vollmer:** Investigation; supervision. **Joe Gray:** Investigation. **Waldemar Vollmer:** Supervision; writing – review and editing; funding acquisition; methodology. **Joseph A. Sorg:** Funding

acquisition; writing – review and editing; supervision; methodology. **Paula S. Salgado:** Funding acquisition; writing – review and editing; supervision; methodology. **Adriano O. Henriques:** Conceptualization; writing – review and editing; supervision; funding acquisition; methodology. **Mónica Serrano:** Funding acquisition; conceptualization; writing – review and editing; investigation; supervision; project administration; formal analysis; methodology.

## ACKNOWLEDGMENTS

This work was supported by the European Union Marie Sklodowska Curie Innovative Training Networks (contract number 642068) to AOH and AF was the recipient of a PhD fellowship under that contract. This project was supported by award PTDC/BIA-MIC/29293/2017 to MS. This work was also financially supported by Project LISBOA-01-0145-FEDER-007660 ("Microbiologia Molecular, Estrutural e Celular") funded by FEDER funds through COMPETE2020—"Programa Operacional Competitividade e Internacionalização" (POCI), by national funds through the FCT ("Fundação para a Ciência e a Tecnologia"). DM is the recipient of a PhD fellowship (PD/BD/143148/2019) within the scope of the PhD program INTERFACE funded by FCT. This project was supported by the Medical Research Council (grant number MR/V032151/1) awarded to PSS and ABS and the BBSRC (BB/W005557/1, BB/W013630/1) to WV. CGR is supported by a Barbour Foundation PhD Studentship from Faculty of Medical Science, Newcastle University. This project was also supported by awards R01AI116895 and R01AI172043 from the National Institute of Allergy and Infectious Diseases to JAS. The content is solely the responsibility of the authors and does not necessarily represent the official views of the NIAID. The funders had no role in study design, data collection, and interpretation, or the decision to submit the work for publication.

## CONFLICT OF INTEREST STATEMENT

The authors declare no conflict of interest.

## DATA AVAILABILITY STATEMENT

The data that support the findings of this study are available from the corresponding author upon reasonable request.

## ETHICS STATEMENT

The manuscript does not contain human studies or experiments using animals or animal cells.

## ORCID

*Joseph A. Sorg* https://orcid.org/0000-0001-7822-2656
*Paula S. Salgado* https://orcid.org/0000-0003-0417-7615
*Adriano O. Henriques* https://orcid.org/0000-0003-4292-4802
*Mónica Serrano* https://orcid.org/0000-0003-3335-3219

## REFERENCES

Abecasis, A.B., Serrano, M., Alves, R., Quintais, L., Pereira-Leal, J.B. & Henriques, A.O. (2013) A genomic signature and the identification of new sporulation genes. *Journal of Bacteriology*, 195, 2101–2115.

Abt, M.C., McKenney, P.T. & Pamer, E.G. (2016) *Clostridium difficile* colitis: pathogenesis and host defence. *Nature Reviews Microbiology*, 14, 609–620.

Browne, H.P., Forster, S.C., Anonye, B.O., Kumar, N., Neville, B.A., Stares, M.D. et al. (2016) Culturing of 'unculturable' human microbiota reveals novel taxa and extensive sporulation. *Nature*, 533, 543–546.

Campo, N. & Rudner, D.Z. (2006) A branched pathway governing the activation of a developmental transcription factor by regulated intramembrane proteolysis. *Molecular Cell*, 23, 25–35.

Chiba, S., Coleman, K. & Pogliano, K. (2007) Impact of membrane fusion and proteolysis on SpoIIQ dynamics and interaction with SpoIIIAH. *The Journal of Biological Chemistry*, 282, 2576–2586.

Chueh, C.-K., Som, N., Ke, L.-C., Ho, M.-R., Reddy, M. & Chang, C.-I. (2019) Structural basis for the differential regulatory roles of the PDZ domain in C-terminal processing proteases. *MBio*, 10, e01129-19.

De Hoon, M.J.L., Eichenberger, P. & Vitkup, D. (2010) Hierarchical evolution of the bacterial sporulation network. *Current Biology*, 20, R735–R745.

Deakin, L.J., Clare, S., Fagan, R.P., Dawson, L.F., Pickard, D.J., West, M.R. et al. (2012) The *Clostridium difficile spo0A* gene is a persistence and transmission factor. *Infection and Immunity*, 80, 2704–2711.

Dembek, M., Kelly, A., Barwinska-Sendra, A., Tarrant, E., Stanley, W.A., Vollmer, D. et al. (2018) Peptidoglycan degradation machinery in *Clostridium difficile* forespore engulfment. *Molecular Microbiology*, 110, 390–410.

Doan, T., Coleman, J., Marquis, K.A., Meeske, A.J., Burton, B.M., Karatekin, E. et al. (2013) FisB mediates membrane fission during sporulation in *Bacillus subtilis*. *Genes & Development*, 27, 322–334.

Doan, T., Marquis, K.A. & Rudner, D.Z. (2005) Subcellular localization of a sporulation membrane protein is achieved through a network of interactions along and across the septum. *Molecular Microbiology*, 55, 1767–1781.

Doan, T. & Rudner, D.Z. (2007) Perturbations to engulfment trigger a degradative response that prevents cell-cell signalling during sporulation in *Bacillus subtilis*: engulfment defects trigger a degradative response. *Molecular Microbiology*, 64, 500–511.

Dong, T.C. & Cutting, S.M. (2004) The PDZ domain of the SpoIVB transmembrane signaling protein enables cis-trans interactions involving multiple partners leading to the activation of the pro-σK processing complex in *Bacillus subtilis*. *Journal of Biological Chemistry*, 279, 43468–43478.

Eichenberger, P., Fujita, M., Jensen, S.T., Conlon, E.M., Rudner, D.Z., Wang, S.T. et al. (2004) The program of gene transcription for a single differentiating cell type during sporulation in *Bacillus subtilis*. *PLoS Biology*, 2, e328.

Emsley, P. & Cowtan, K. (2004) *Coot*: model-building tools for molecular graphics. *Acta Crystallographica. Section D, Biological Crystallography*, 60, 2126–2132.

Fimlaid, K.A., Bond, J.P., Schutz, K.C., Putnam, E.E., Leung, J.M., Lawley, T.D. et al. (2013) Global analysis of the sporulation pathway of *Clostridium difficile*. *PLoS Genetics*, 9, e1003660.

Fimlaid, K.A., Jensen, O., Donnelly, M.L., Siegrist, M.S. & Shen, A. (2015) Regulation of *Clostridium difficile* spore formation by the SpoIIQ and SpoIIIA proteins. *PLoS Genetics*, 11, e1005562.

Galperin, M.Y., Mekhedov, S.L., Puigbo, P., Smirnov, S., Wolf, Y.I. & Rigden, D.J. (2012) Genomic determinants of sporulation in Bacilli and Clostridia: towards the minimal set of sporulation-specific genes. *Environmental Microbiology*, 14, 2870–2890.

Gil, F., Lagos-Moraga, S., Calderón-Romero, P., Pizarro-Guajardo, M. & Paredes-Sabja, D. (2017) Updates on *Clostridium difficile* spore biology. *Anaerobe*, 45, 3–9.

Hara, H., Yamamoto, Y., Higashitani, A., Suzuki, H. & Nishimura, Y. (1991) Cloning, mapping, and characterization of the *Escherichia coli prc* gene, which is involved in C-terminal processing of penicillin-binding protein 3. *Journal of Bacteriology*, 173, 4799–4813.

Harish, B.S. & Uppuluri, K.B. (2018) Microbial serine protease inhibitors and their therapeutic applications. *International Journal of Biological Macromolecules*, 107, 1373–1387.

Henriques, A.O., Melsen, L.R. & Moran, C.P. (1998) Involvement of superoxide dismutase in spore coat assembly in *Bacillus subtilis*. *Journal of Bacteriology*, 180, 2285–2291.

Henriques, A.O. & Moran, C.P. (2007) Structure, assembly, and function of the spore surface layers. *Annual Review of Microbiology*, 61, 555–588.

Hilbert, D.W. & Piggot, P.J. (2004) Compartmentalization of gene expression during *Bacillus subtilis* spore formation. *Microbiology and Molecular Biology Reviews: MMBR*, 68, 234–262.

Hoa, N.T., Brannigan, J.A. & Cutting, S.M. (2001) The PDZ domain of the SpoIVB serine peptidase facilitates multiple functions. *Journal of Bacteriology*, 183, 4364–4373.

Hoa, N.T., Brannigan, J.A. & Cutting, S.M. (2002) The *Bacillus subtilis* signaling protein SpoIVB defines a new family of serine peptidases. *Journal of Bacteriology*, 184(1), 191–199.

Horsburgh, G.J., Atrih, A. & Foster, S.J. (2003) Characterization of LytH, a differentiation-associated peptidoglycan hydrolase of *Bacillus subtilis* involved in endospore cortex maturation. *Journal of Bacteriology*, 185, 3813–3820.

Jiang, X., Rubio, A., Chiba, S. & Pogliano, K. (2005) Engulfment-regulated proteolysis of SpoIIQ: evidence that dual checkpoints control $\sigma^K$ activity. *Molecular Microbiology*, 58, 102–115.

Jumper, J., Evans, R., Pritzel, A., Green, T., Figurnov, M., Ronneberger, O. et al. (2021) Highly accurate protein structure prediction with AlphaFold. *Nature*, 596, 583–589.

Kelly, A. & Salgado, P.S. (2019) The engulfasome in *C. difficile*: variations on protein machineries. *Anaerobe*, 60, 102091.

Khanna, K., Lopez-Garrido, J. & Pogliano, K. (2020) Shaping an endospore: architectural transformations during *Bacillus subtilis* sporulation. *Annual Review of Microbiology*, 74, 361–386.

Kuru, E., Lambert, C., Rittichier, J., Till, R., Ducret, A., Derouaux, A. et al. (2017) Fluorescent D-amino-acids reveal bi-cellular cell wall modifications important for *Bdellovibrio bacteriovorus* predation. *Nature Microbiology*, 2, 1648–1657.

Londoño-Vallejo, J.A., Fréhel, C. & Stragier, P. (1997) SpoIIQ, a forespore-expressed gene required for engulfment in *Bacillus subtilis*. *Molecular Microbiology*, 24, 29–39.

Martins, D., DiCandia, M.A., Mendes, A.L., Wetzel, D., McBride, S.M., Henriques, A.O. et al. (2021) CD25890, a conserved protein that modulates sporulation initiation in *Clostridioides difficile*. *Scientific Reports*, 11(1), 7887.

Mastny, M., Heuck, A., Kurzbauer, R., Heiduk, A., Boisguerin, P., Volkmer, R. et al. (2013) CtpB assembles a gated protease tunnel regulating cell-cell signaling during spore formation in *Bacillus subtilis*. *Cell*, 155, 647–658.

Mirdita, M., Schütze, K., Moriwaki, Y., Heo, L., Ovchinnikov, S. & Steinegger, M. (2022) ColabFold: making protein folding accessible to all. *Nature Methods*, 19, 679–682.

Muley, V.Y., Akhter, Y. & Galande, S. (2019) PDZ domains across the microbial world: molecular link to the proteases, stress response, and protein synthesis. *Genome Biology and Evolution*, 11, 644–659.

Nerber, H.N., Baloh, M. & Sorg, J.A. (2023) The small acid-soluble proteins of *Clostridioides difficile* regulate sporulation in a SpoIVB2-dependent manner. *bioRxiv*. 541253. Available from: https://doi.org/10.1101/2023.05.17.541253. Preprint.

Nerber, H.N. & Sorg, J.A. (2021) The small acid-soluble proteins of *Clostridioides difficile* are important for UV resistance and serve as a check point for sporulation. *PLoS Pathogens*, 17(9), e1009516.

Ng, Y.K., Ehsaan, M., Philip, S., Collery, M.M., Janoir, C., Collignon, A. et al. (2013) Expanding the repertoire of gene tools for precise manipulation of the *Clostridium difficile* genome: allelic exchange using *pyrE* alleles. *PLoS One*, 8, e56051.

Oke, V., Shchepetov, M. & Cutting, S. (1997) SpoIVB has two distinct functions during spore formation in *Bacillus subtilis*. *Molecular Microbiology*, 23, 223–230.

Olenic, S., Heo, L., Feig, M. & Kroos, L. (2022) Inhibitory proteins block substrate access by occupying the active site cleft of *Bacillus subtilis* intramembrane protease SpoIVFB. *eLife*, 11, e74275.

Pan, Q., Losick, R. & Rudner, D.Z. (2003) A second PDZ-containing serine protease contributes to activation of the sporulation transcription factor sigmaK in *Bacillus subtilis*. *Journal of Bacteriology*, 185, 6051–6056.

Pazos, M., Peters, K. & Vollmer, W. (2017) Robust peptidoglycan growth by dynamic and variable multi-protein complexes. *Current Opinion in Microbiology*, 36, 55–61.

Pereira, F.C., Saujet, L., Tomé, A.R., Serrano, M., Monot, M., Couture-Tosi, E. et al. (2013) The spore differentiation pathway in the enteric pathogen *Clostridium difficile*. *PLoS Genetics*, 9, e1003782.

Putnam, E.E., Nock, A.M., Lawley, T.D. & Shen, A. (2013) SpoIVA and SipL are *Clostridium difficile* spore morphogenetic proteins. *Journal of Bacteriology*, 195, 1214–1225.

Ramírez-Guadiana, F.H., Rodrigues, C.D.A., Marquis, K.A., Campo, N., Barajas-Ornelas, R.D.C., Brock, K. et al. (2018) Evidence that regulation of intramembrane proteolysis is mediated by substrate gating during sporulation in *Bacillus subtilis*. *PLoS Genetics*, 14(11), e1007753.

Ribis, J.W., Fimlaid, K.A. & Shen, A. (2018) Differential requirements for conserved peptidoglycan remodeling enzymes during *Clostridioides difficile* spore formation. *Molecular Microbiology*, 110, 370–389.

Rodrigues, C.D.A., Marquis, K.A., Meisner, J. & Rudner, D.Z. (2013) Peptidoglycan hydrolysis is required for assembly and activity of the transenvelope secretion complex during sporulation in *Bacillus subtilis*. *Molecular Microbiology*, 89, 1039–1052.

Rosenbusch, K.E., Bakker, D., Kuijper, E.J. & Smits, W.K. (2012) *C. difficile* 630Δ*erm* Spo0A regulates sporulation, but does not contribute to toxin production, by direct high-affinity binding to target DNA. *PLoS One*, 7, e48608.

Saujet, L., Pereira, F.C., Serrano, M., Soutourina, O., Monot, M., Shelyakin, P.V. et al. (2013) Genome-wide analysis of cell type-specific gene transcription during spore formation in *Clostridium difficile*. *PLoS Genetics*, 9, e1003756.

Serrano, M., Crawshaw, A.D., Dembek, M., Monteiro, J.M., Pereira, F.C., Pinho, M.G. et al. (2016) The SpoIIQ-SpoIIIAH complex of *Clostridium difficile* controls forespore engulfment and late stages of gene expression and spore morphogenesis. *Molecular Microbiology*, 100, 204–228.

Serrano, M., Kint, N., Pereira, F.C., Saujet, L., Boudry, P., Dupuy, B. et al. (2016) A recombination directionality factor controls the cell type-specific activation of $\sigma^K$ and the fidelity of spore development in *Clostridium difficile*. *PLoS Genetics*, 12, e1006312.

Setlow, P. & Christie, G. (2023) New thoughts on an old topic: secrets of bacterial spore resistance slowly being revealed. *Microbiology and Molecular Biology Reviews*, 87, e0008022.

Singh, S.K., Parveen, S., SaiSree, L. & Reddy, M. (2015) Regulated proteolysis of a cross-link–specific peptidoglycan hydrolase contributes to bacterial morphogenesis. *Proceedings of the National Academy of Sciences of the United States of America*, 112, 10956–10961.

Smits, W., Browne, H.P., Choudhary, J.S., Dougan, G., Lawley, T.D., Martin, M.J. et al. (2014) Functional genomics reveals that *Clostridium difficile* Spo0A coordinates sporulation, virulence and metabolism. *BMC Genomics*, 15, 160.

Smits, W.K., Lyras, D., Lacy, D.B., Wilcox, M.H. & Kuijper, E.J. (2016) *Clostridium difficile* infection. *Nature Reviews Disease Primers*, 2, 16020.

Sun, G., Yang, M., Jiang, L. & Huang, M. (2021) Regulation of pro-σK activation: a key checkpoint in *Bacillus subtilis* sporulation. *Environmental Microbiology*, 23, 2366–2373.

Traag, B.A., Pugliese, A., Eisen, J.A. & Losick, R. (2013) Gene conservation among endospore-forming bacteria reveals additional sporulation genes in *Bacillus subtilis*. *Journal of Bacteriology*, 195, 253–260.

van Kempen, M., Kim, S.S., Tumescheit, C., Mirdita, M., Gilchrist, C.L.M., Söding, J. et al. (2024) Fast and accurate protein structure search with Foldseek. *Nat Biotechnol*. 42, 243–246. Available from: https://doi.org/10.1038/s41587-023-01773-0

Wakeley, P.R., Dorazi, R., Hoa, N.T., Bowyer, J.R. & Cutting, S.M. (2000) Proteolysis of SpoIVB is a critical determinant in signalling of pro-sigmaK processing in *Bacillus subtilis*. *Molecular Microbiology*, 36, 1336–1348.

Xie, X., Guo, N., Xue, G., Xie, D., Yuan, C., Harrison, J. et al. (2019) Solution structure of SpoIVB reveals mechanism of PDZ domain-regulated protease activity. *Frontiers in Microbiology*, 10, 1232.

Zhou, R. & Kroos, L. (2005) Serine proteases from two cell types target different components of a complex that governs regulated intramembrane proteolysis of pro-sigmaK during *Bacillus subtilis* development. *Molecular Microbiology*, 58, 835–846.

## SUPPORTING INFORMATION

Additional supporting information can be found online in the Supporting Information section at the end of this article.

**How to cite this article:** Martins, D., Nerber, H.N., Roughton, C.G., Fasquelle, A., Barwinska-Sendra, A., Vollmer, D. et al. (2024) Cleavage of an engulfment peptidoglycan hydrolase by a sporulation signature protease in *Clostridioides difficile*. *Molecular Microbiology*, 00, 1–17. Available from: https://doi.org/10.1111/mmi.15291